Marked-up manuscript version

Centennial to millennial climate variability in the far northwestern Pacific (off Kamchatka) and its linkage to the East Asian monsoon and North Atlantic from the Last Glacial Maximum to the Early Holocene

Sergey A. Gorbarenko [1], Xuefa Shi [2, 3], Min-Te Chen [4], Galina Yu. Malakhova, [5],

Aleksandr A. Bosin [1], Yanguang Liu [2, 3], Jianjun Zou [2, 3]

[1] V.I. Il'ichev Pacific Oceanological Institute, Russia

[2] Key Laboratory of Marine Sedimentology and Environmental Geology, First Institute of Oceanography, SOA, Qingdao, China

[3] Laboratory for Marine Geology, Qingdao National Laboratory for Marine Science and Technology, Qingdao, China

[4] National Taiwan Ocean University

[5] North-East Interdisciplinary Science Research Institute FEB RAS, Russia

Abstract

High resolution reconstructions based on productivity proxies and magnetic properties of core LV63-41-2 (off Kamchatka) reveal prevailing centennial productivity/climate variability in the northwestern (NW) Pacific from the Last Glacial Maximum (LGM) to the Early Holocene (EH). The age model of the core is established by AMS ^{14}C dating and by projections of AMS ^{14}C data of the nearby core SO-201-12KL through correlation of the productivity proxies and relative paleomagnetic intensity. Resulted sequence of centennial productivity increases/climate warming events in the NW Pacific occurred synchronously with the East Asian Summer Monsoon (EASM) sub-interstadials during the LGM (4 events), Heinrich Event 1 (HE1) (4 events), Bølling/Allerød (B/A) warming (4 events), and over the EH (4 events). Remarkable similarity of the sequence of the NW Pacific increased productivity events with the EASM sub-interstadials over the LGM-HE1 implies that Siberian High is a strong common driver responded to the variations in productivity and sub-interstadial. The comparison with the $\delta^{18}O$ record from Antarctica suggests that, another mechanism associated with temperature gradient in the Southern Hemisphere may be also responded for the EASM / NW Pacific centennial events over the LGM-HE1. During the B/A warming and resumption of the AMOC, clear synchronicity between the NW Pacific, EASM and Greenland sub-interstadials was mainly controlled by changes in the atmospheric circulation. During the EH the linkages between sun-ocean-climate, likely, control the synchronicity of abrupt

climate changes in the NW Pacific and North Atlantic. The sequence of centennial events recorded in this study is a persistent regional feature during the LGM-EH, which may serve as a template in high resolution paleoceanography and sediment stratigraphy in the NW Pacific.

1. Introduction

Model simulations and proxy-based records both have led to contradictory results on the millennial-scale environmental variability in the northwestern (NW) Pacific and its underlying mechanisms during the last deglaciation. These model and proxy studies suggested either in-phase relationships of deglacial variability between the North (N) Atlantic and NW Pacific (Caissie et al., 2010; Chikamoto et al., 2012; Kienast and McKay, 2001; Seki et al., 2002) or out-of-phase responses (Gebhardt et al., 2008; Sarnthein et al., 2006). The in phase relationship has been attributed to rapid atmospheric teleconnections in the Northern Hemisphere on a decadal time scale (Max et al., 2012). The winter Arctic Oscillation (AO), which resembles the North Atlantic Oscillation, directly influences the surface air temperature and sea level pressure over the region northwards of 35ºN in East Asia (Sung et al., 2006). The Siberian High (SH), an essential component of northern East Asian atmosphere system, significantly influences the East Asian Winter Monsoon (EAWM) (Wu and Wang, 2002), which in turn affect the environment of NW Pacific. When winter AO is in its positive phase, both winter SH and EAWM are weaker than their normal state and air temperature of the surface- the middle troposphere is higher than normal (Wu and Wang, 2002), which ameliorate the NW Pacific environment. The out-of-phase response, however, was proposed to be driven by a seesaw mechanism, with oceanic readjustments between the weakening of the Atlantic meridional overturning circulation (AMOC) and the strengthening of the Pacific meridional overturning circulation (Okazaki et al., 2010).

Records of $\delta^{18}O$ from the Greenland ice cores revealed the Dansgaard - Oeschger (DO) millennial scale oscillations (interstadials and stadials) during the last glaciation (Dansgaard et al., 1993; Johnsen et al., 1992) and similar millennial scale events have also been identified in a number of terrestrial and marine records in other regions. For example, a synthesis of the last glacial pollen records from the European continent provides evidence that the warmer intervals in Europe correspond to millennial-scale interstadials in Greenland (Fletcher et al., 2010). The sediment cores from the N Pacific and its marginal seas also showed abrupt, millennial scale climate and environment ameliorations, similar to interstadials in Greenland ice cores during the last glaciation. Records of $\delta^{18}O$ of planktic foraminifera (Kennett et al., 2000) and alkenone-derived sea surface temperature (SST) (Seki et al., 2002) from the Northeastern (NE) Pacific also exhibited millennial climate oscillations very similar in magnitude with DO cycles over the last glaciation. INTIMATE stratigraphy studies introduced the subdivision of the GI-1 into sub-interstadials GI-1a to GI-1e.

Furthermore, the GS-2.1 was subdivided into sub-stadials GS-2.1a (during Heinrich Event 1, HE1), GS-2.1b (Last Glacial Maximum, LGM), and GS-2.1c (Björck et al., 1998; Rasmussen et al., 2014). The sequence of abrupt warming and environmental ameliorations similar to DO interstadials in Greenland were also interpreted by using alkenone-derived SST (Harada et al., 2008) and geochemical, diatom and pollen data (Gorbarenko et al., 2004) in sediment cores investigated from the Okhotsk Sea. The Bering Sea was also characterized by climate and environmental oscillations corresponded to DO cycles based on productivity proxies, sediment density, opal content and micropaleontological records (Gorbarenko et al., 2005; Kim et al., 2011; Riethdorf et al., 2013; Schlung et al., 2013).

By comparing the dust content in the North Greenland Ice Core Project (NGRIP) ice core with that of the dust record in a sediment core from the subarctic N Pacific, Serno et al. (2015) demonstrated synchronicity of millennial scale changes in atmospheric circulation between the N Pacific and the Greenland during the last 27 ka (Serno et al., 2015). Previous studies also found the occurrence of increased export of productivity during the period of millennial scale climate and environmental ameliorations, correlated with DO interstadials, in the Okhotsk and Bering Seas (Gorbarenko et al., 2005; Kim et al., 2011; Riethdorf et al., 2013; Seki et al., 2004).

Recent studies on high-resolution and well-dated sediment cores from the subarctic NW Pacific, the Okhotsk Sea, and the western Bering Sea show the variations in SST during the last deglaciation similar to the NE Pacific and to the N Atlantic and Greenland temperature variability (Caissie et al., 2010; Max et al., 2012; Seki et al., 2002). These studies suggest a close linkage to deglacial variations in AMOC associated with rapid atmospheric teleconnection, which were responsible for a quasi-synchronous SST pattern between the N Atlantic and N Pacific during the last deglaciation.

Furthermore, a recent study by Praetorius and Mix (2014), based on multi-decadal-resolution foraminiferal $\delta^{18}O$ records from the Gulf of Alaska, revealed a synchronicity of rapid climate shifts between the N Atlantic/Greenland (NGRIP record) and the NE Pacific between 15.5 and 11 ka. During the Holocene and HE1, inverse relationships between the N Atlantic and the N Pacific are suggested by Praetorius and Mix (2014), while the short-term variability is either not sufficiently resolved or decoupled.

A lack of high resolution records in the NW Pacific prohibits a precise assessment of any possible climatic teleconnection between the N Pacific and N Atlantic.

Besides centennial-millennial oscillations reported during the last glacial periods, centennial precipitation anomalies from LGM to the Holocene have also been reported in cave stalagmite $\delta^{18}O$

records of the East Asian monsoon (Dykoski et al., 2005; Wang et al., 2001, 2005, 2008; Yuan et al., 2004). Furthermore, the timing and pattern of variability during the Early Holocene (EH) regional climate changes are still under debate. In particular, though the EH climate has started from a strong warming in most cases, a Hani peat $\delta^{18}O$ record from NE China instead suggest centennial cooling event which is primarily superimposed on a long-term warming trend during the Holocene (Hong et al., 2009).

Here we present high resolution results of productivity proxies, sediment magnetic properties, and lithological composition of a sediment core LV 63-41-2 (hereinafter, 41-2) (off Kamchatka) from the NW Pacific. Our records reveal a sequence of centennial productivity/climate variability from 20 ka to 8 ka. An age model of core 41-2 was constructed using accelerator mass spectrometry (AMS) ^{14}C dating and by correlating the productivity events and relative paleomagnetic intensity (RPI) variability with those of the well-dated nearby core SO-201-12KL (hereinafter, 12KL) (Max et al., 2012, 2014). Using robust age controls, we establish a tight linkage between the centennial events with higher productivity in the NW Pacific and the sub-interstadial strengthened East Asian summer monsoon (EASM) expressed in cave stalagmite $\delta^{18}O$ records. These results enable further investigation of any mechanisms in controlling the in phase relationships of the centennial variability in the NW Pacific / EASM and those underlying the Greenland / N Atlantic and Antarctic climate changes during the LGM through EH.

2 Materials and methods

Sediment core 41-2 (52°34′ N, 160°01′ E; water depth: 1924 m) was recovered from the NW Pacific off Kamchatka Peninsula during the Russian-Chinese Joint Expedition on R/V "Akademik M.A. Lavrentyev" in 2013. The length of the core is 467 cm. In order to establish the age model of core 41-2, we also analyzed paramagnetic magnetization and chlorin content in core 12KL (53°59′ N, 162°23′ E), which has been dated well by Max et al. (2012, 2014).

2.1 Coarse fraction

The weight percentage of coarse fraction (CF; 63-2000 μm) was obtained at 1 cm interval after wet sieving the sediment and calculated as a ratio of CF weight to the total weight of dry bulk sediment.

Terrigenous materials are mainly transported by sea ice in the studied region and therefore the CF and magnetic susceptibility (MS) of sediments (Gorbarenko et al., 2003, 2012; Lisitzin, 2002; Sakamoto et al., 2005), can be used as a proxy for ice rafted debris (IRD). Semi-quantitative estimates of terrigenous and volcanic particles (tephra) in the CF allow the determination of core intervals with insignificant amounts of tephra, and therefore intervals with implications for CF and

MS as an IRD index. Semi-quantitative estimates of major components in the sediment CF, including terrigenous and volcanic particles, benthic and planktic foraminifera shells, diatom frustules, and radiolarian skeletons on a twelve-point scale, were made by using a microscope for roughly estimating the proportions of different components in the sediment (Rothwell, 1989).

2.2 Chlorin

Chlorin content is assumed to reflect changes in primary surface ocean productivity, because continental-derived chlorophyll contributes insignificantly to its composition in deep marine sediment (Harris et al., 1996). The chlorin content in core 41-2 was measured by a Shimadzu UV-1650PC spectrophotometer at 1 cm resolution, and at 2 cm resolution in core 12KL, respectively, using same analytical reagents and pretreatment procedures proposed by Harris et al. (1996).

2.3 Total organic carbon (TOC), calcium carbonate ($CaCO_3$), and color b*

Contents of TOC, $CaCO_3$, and biogenic opal in deep sea sediments are usually used as key parameters to assess paleoproductivity (Berger et al., 1989; Narita et al., 2002; Prahl et al., 1989; Seki et al., 2004). The color b* values correlate well with the changes in biogenic opal content in sediment cores (Nürnberg and Tiedemann, 2004) and are widely used as a paleoproductivity proxy in the NW Pacific and its marginal seas (Gorbarenko et al., 2012; Max et al., 2012; Riethdorf et al., 2013).

Total carbon and inorganic carbon contents in core 41-2 were measured at every 2 cm throughout the core by Coulometry using an AN-7529 analyzer (Gorbarenko et al., 1998). TOC content was determined by calculating the difference between total carbon and inorganic carbon content. Color b* index (psychometric yellow–blue chromaticness) was measured with 1 cm resolution using a Minolta CM-2002 color reflectance spectrophotometer (Harada, 2006).

2.4 Radiocarbon dating (AMS ^{14}C)

AMS ^{14}C-ages were measured in monospecific samples of the planktic foraminifera *Neogloboquadrina pachyderma* sinistral (*N. pachyderma* sin.) from the 125–250 μm fraction, and benthic foraminifera *Epistominella pacifica*, and *Uvigerina parvocostata* from the 250–350μm fraction of the core. The radiocarbon dating was performed by Dr. John Southon at the Keck Carbon Cycle AMS Facility (UCIAMS) in the Earth System Science Department of the University of California, USA.

The constant reservoir age (900 ± 250 yr) of the NW Pacific surface water (Max et al., 2012) was adopted in this study to convert the ^{14}C data into calendar ages by using Calib Rev 6.0 (Stuiver and Reimer, 1993) with Marine13 calibration curve (Reimer et al., 2013) to establish consistent

AMS ^{14}C chronologies between cores 41-2 and 12KL. When using benthic foraminifera for AMS ^{14}C dating on the cores, an age difference of 1400 yrs is taken between coexisting benthic and planktic foraminifera ages (Max et al., 2014).

2.5 Magnetic properties

RPI in response to variations in the Earth's magnetic field presents an independent chronological instrument of marine and continental sediments (Channell et al., 2009), and are widely used for sediment correlation and chronology determination (Kiefer et al., 2001; Riethdorf et al., 2013). The sediment paramagnetic magnetization (PM) was formed in marine sediments in the open NW Pacific by silicate, paramagnetic iron sulphide (FeS), and fine clay minerals, the main part of which was transported from land as an eolian dust through atmospheric circulation by westerly jets (Serno et al., 2015). Therefore, the sediment PM may serve as a proxy for the land aridity and atmosphere circulation pattern changes in response to climate change. The volume MS of sediments was mainly formed by ferromagnetic minerals delivered together with terrigenous materials from adjacent land by sea ice, which is the main transport agent of clastic materials into the NW Pacific and its marginal seas (Gorbarenko et al., 2003; Lisitzin, 2002; Sakamoto et al., 2005).

The sediment magnetic properties were measured at 2.2 cm resolution in cores 41-2 and 12KL. MS of these samples was measured by an AGICO MFK1-FA device. The characteristic of remanent magnetization (ChRM) of the samples was measured in the same way by studying the stability of natural remanent magnetization (NRM) in an alternative magnetic fields of up to 80-100 mT on the basis of analysis of Zijderveld vector plots, using an AGICO LDA-3Adevice and rock-generator AGICO JR-5a (Zijderveld, 1964). The module and direction of NRM were measured on a JR-5A rock-generator after the stepwise demagnetization of reference samples by alternating magnetic fields with vanishing amplitude (Malakhov et al., 2009). Ahysteretic remanent magnetization (ARM) was generated using an AGICO AMU-1A device and measured using the JR-5A rock-generator. The RPI of the studied core was determined by the normalization of the ChRM after demagnetization at 20 mT by ARM (ChRM/ARM) (Tauxe, 1993). The sediment PM was measured for each sample from curves of magnetic hysteresis by a J Meter coercitive spectrometer at Kazan State University, Kazan, Russia (Enkin et al., 2007; Jasonov et al., 1998).

2.6 In-situ X‐ray fluorescence core scanning

Previous studies have shown that the non-destructive, high resolution X-ray fluorescence (XRF) measurements of biogenic barium, bromine and silica (Ba-bio, Br-bio, and Si-bio, respectively) by a core scanner or synchrotron radiation are consistent with analytically measured

contents of Ba-bio, TOC, and biogenic opal, respectively, and therefore may be used as paleoproductivity proxies (Goldberg et al., 2005; Nürnberg and Tiedemann, 2004; Riethdorf et al., 2016). Ba-bio is formed during the decay of organic matter in the water column and the uptake of Ba in settling particles (Dymond et al., 1992), and has been previously used as a proxy of productivity (Goldberg and Arrhenius, 1958; McManus et al., 1998). Si-bio, related with biogenic opal in deep sea sediments, is usually used as a key parameter to assess paleoproductivity (Berger et al., 1989; Narita et al., 2002; Seki et al., 2004). Br-bio content measured using a core scanner is strongly correlated with TOC variability (Riethdorf et al., 2013) and therefore may also be used as a paleoproductivity proxy.

The elemental composition of core 41-2 was measured as peak area in counts per second at 0.5 cm resolution using the Itrax XRF core scanner at the First Institute of Oceanography, State Oceanic Administration, China. The Itrax XRF core scanner was set at 20 s count times, 30 kV X-ray voltage, and an X-ray current of 20 mA. Though absolute elemental concentrations are not directly available from the micro-XRF measurements, the count values can be used as estimates of the relative concentrations. The count values may be influenced by changes in the physical properties of the sediment, such as the water content and surface roughness of the core (Röhl and Abrams, 2000). However, the grain size of the 41-2 core is rather fine and the surface has been processed to be as flat as possible to minimize any effects from changing physical properties or roughness during the scanning.

In this study, attention was paid to the XRF scanning results for estimating the productivity proxies such as Ba-bio, Br-bio and Si-bio contents in our sediment core. The content of Ba-bio was estimated by the subtraction of its terrigenous component from the total Ba concentration in sediment (Ba-tot). The terrigenous component was, in turn, calculated from empirical regional $(Ba/Al)_{ter}$ ratios in the sediment core with the lowest Ba-tot contents multiplied on relative Al content:

Ba-bio = Ba-tot – $(Ba/Al)_{ter}$*Al (Goldberg et al., 2005).

The contents of Br-bio and Si-bio were calculated using the same way.

3. Results

3.1 Productivity events

Down-core variability of all productivity proxies (color b*and contents of TOC, chlorin, $CaCO_3$, Ba-bio, Si-bio, and Br-bio) in core 41-2 is presented Fig. 2. Taking the available AMS ^{14}C data into account (Table 1), the middle part of the core (the interval ~315-230 cm) with increased

contents/values of all productivity proxies could be chronologically assigned to the Bølling/Allerød (B/A) warming right after the late last glaciation (467-315 cm) consistently with current investigations. The climate became warmer in the northern extra-tropics during the B/A period, terminating the last glaciation, then it reversed to the cooling during the Younger Dryas (YD) followed by the significant warming throughout the Holocene. This climate sequence had been well-documented by the $\delta^{18}O$ records of the Greenland ice cores and climate records from the N Atlantic (Bond et al., 2001; Dansgaard et al., 1993; Johnsen et al., 1992; Stuiver et al., 1995), by classical sequence of European pollen zone (Nilsson, 1983) and by well-dated pollen biome records of the southern Siberia (Bezrukova et al., 2010; Tarasov et al., 2009). Above mentioned patterns of climate variability during the LGM–EH in moderate-high latitudes of the Northern Hemisphere is consistent with the N Pacific and its marginal seas, evidenced by the alkenone- derived SST (Barron et al., 2003; Max et al., 2012) and pollen records (Gorbarenko et al., 2003, 2004). The significant increase in productivity during the B/A was likely achieved by additional nutrient input into euphotic layer due to accelerated sea level rise (Siddall et al., 2010) accompanied by the supply of organic matter from the submerged shelf and by prolonged blooming season due to the warming that is a common paleoceanography feature of the N Pacific and its marginal seas (Barron et al., 2003, 2009; Caissie et al., 2010; Galbraith et al., 2007; Gorbarenko, 1996; Gorbarenko et al., 2005; Gorbarenko and Goldberg, 2005; Keigwin, 1998; Keigwin et al., 1992; Max et al., 2012; Seki et al., 2004). A decreased trend of productivity records at the interval of~230-190 cm is likely associated with the YD cooling and the subsequent high productivity trend in the upper 190 cm of the core is presumably related to the Holocene warming (Fig. 2).

In core 41-2, the temporal resolutions of measured color b*, chlorin, TOC, $CaCO_3$ and magnetic parameters (PM, MS, and RPI), and Ba-bio, Br-bio, and Si-bio are nearly 30 years, 15 years, and 60 years respectively. The resolution is high enough to allow us to detect the centennial scale productivity variability in the NW Pacific. However, not all productivity proxies change synchronously (Fig. 2).

Each used productivity proxy has its own specific limitations and peculiarities in response to the environmental and primary productivity changes. For example, although carbonaceous fossils (planktic foraminifera and coccolithophorids) rain from the euphotic layer, exported by primary production, and they provide the main carbonate input into the sediment. While the $CaCO_3$ content in the deep sea sediment is mostly governed by climatically forced variability in the deep water chemistry and carbonate ion concentration (CO_3^{2-}), resulting in different carbonate preservation in the past (Yu et al., 2013). As for the Ba-bio proxy, Jaccard et al. (2010) suggest that in the highly productive areas, barite dissolution has been observed under suboxic conditions, precluding its

application as a quantitative proxy to reconstruct past changes in export production. Although it has been suggested that biogenic opal and TOC contents are responsible for the accumulation of siliceous fossils, and siliceous plus carbonaceous fossils with other organic remains, respectively (Berger et al., 1989), they vary in different ways at various periods in sediments of the NW Pacific and its marginal seas. For example, biogenic opal content in the Okhotsk Sea lags significantly relative to TOC changes during the last deglaciation—the Late Holocene interval (Gorbarenko et al., 1998; Seki et al., 2004). TOC content in the hemipelagic sediment includes the organic carbon formed by marine primary production, and the terrigenous organic material delivered from land. Although it was suggested that color b* values correlate well with the changes in biogenic opal content in sediment cores (Nürnberg and Tiedemann, 2004), measured color b* in core 41-2 do not change synchronously with Si-bio content in the entire length of the core (Fig. 2). The presentation of a wide range of productivity records allows us to evaluate the discrepancy among proxies. In addition, the combination of proxies provides a more reliable way for evaluating the productivity changes.

For the statistical assessment of the centennial productivity variability, the stack of productivity proxies is calculated. It is an average of the normalized data of each proxy with equal weight (Fig. 2). Data from the productivity stack were detrended by subtracting long-term periodicity that allow us to determine the sequence of centennial productivity events with higher productivity throughout the studied core and events with lower productivity during the EH based on the seven productivity proxies measured (Fig. 2). Calculated productivity stack has high negative correlation with PM of sediments ($r = -0.63$). This indicates that centennial events with increased productivity occurred during weakening of dust delivery and deposition in the NW Pacific by atmospheric circulation associated with abrupt climate warming. Such causal linkages between centennial productivity increases and abrupt climate warming in the NW Pacific is also consistent with millennial scale productivity /climate oscillation during the DO interstadials found in the Okhotsk and Bering Seas (Gorbarenko et al., 2005; Kim et al., 2011; Riethdorf et al., 2013; Seki et al., 2004). As a result, the records of different productivity proxies and detrended productivity stack show eight short-term events with higher productivity occurred during the LGM and HE1 and 4 events during the B/A warming. During the EH, productivity records show 4 events of lower and higher productivity, respectively (Fig. 2).

It is noted that a low productivity event at ~9.1 ka (Table 1) is well-correlated with the 9.3 ka cold event recorded in NGRIP (Rasmussen et al., 2014). Moreover, a low productivity event identified at depth of 105-110 cm also correspond to the 8.2 ka cold event, a well-known chronostratigraphic marker in the Early to Middle Holocene boundary (Walker et al., 2012).

3.2. Age model

The RPI, productivity stack and PM of core 41-2 were compared with the RPI, several productivity proxies, and PM records of nearby core 12KL (Fig. 3). The color b* index and Ca (analog of $CaCO_3$ content) of core 12KL were obtained from Max et al. (2012, 2014). The correlation of the centennial productivity events between cores was provided by comparison of productivity stack of core 41-2 with productivity proxies of core 12KL and by comparison of the RPI and PM curves. An age model of core 41-2 was constructed using all available AMS ^{14}C data, with additional age control points identified by correlating the centennial productivity events, RPI and PM of the studied core with those of the well-dated adjacent core 12KL (Max et al., 2012, 2014) (Fig. 3). The age tuning used in this study assumes a synchronous pattern of productivity, RPI and PM variability in the NW Pacific since the last glacial, especially for closely-located cores. Therefore, the centennial variability of productivity proxies with increased productivity events, RPI of Earth's magnetic field, and PM identified in cores 41-2 and 12KL have to be closely matched in both cores over the last glaciation—B/A warming to the EH (Fig. 3). It was noted that the available age model for core 12KL (the Tiedemann/Max age model) (Max et al., 2012, 2014) was based on the AMS ^{14}C data and correlation of color b* index with the NGRIP $\delta^{18}O$ curve. For adopting this age model to Core 41-2, the AMS ^{14}C data of core 12KL were projected to Core 41-2 according to the correlation of related productivity events, RPI and PM (Fig. 3). The color b* minimum in core 12KL at a depth of 706 cm, which correlates with a minimum in the NGRIP $\delta^{18}O$ record at 16.16 ka, is also clearly correlated with the color b* minimum in core 41-2 at a depth of 348 cm (Fig. 3). All correlated AMS ^{14}C data points are also well-matched with the measured RPI curves of both cores (Fig. 3). Our four AMS ^{14}C data are fairly close to the projected ^{14}C data from core 12KL (Table 3) with age differences within ±0.1 ka, confirming the validity of these key point projections. Here the use of ^{14}C data of core 12KL is preferred, because this core has a higher sedimentation rate, and planktic foraminifera for these measurements were picked-up from intervals with higher Ca peaks, aiming to reduce the effect of bioturbation on the precision of age model.

A close temporal correlation of these NW Pacific increased productivity events with sub-interstadials in the EASM becomes apparent after projection of the radiocarbon data of both cores on absolute U-Th dated $\delta^{18}O$ record of Chinese cave stalagmites (Wang et al., 2008) during 20–8 ka (Fig. 3). Such inferred synchronicity of abrupt NW Pacific productivity events and EASM sub-interstadials was used for further tuning of age model. This was achieved by fine-tuning of the increased productivity events with related sub-interstadials of $\delta^{18}O$ Chinese stalagmites at a depth beyond the projected AMS ^{14}C data (Fig. 3; Table 3).

The sequence of centennial events of increased productivity seems to be occurred in phase with decreasing of PM in both cores (Fig. 3), indicating a weakening of eolian dust transportation by atmospheric circulation in the study area due likely to climate warming, analogous with millennial scale forcing of dust transportation into the NW Pacific (Serno et al., 2015). Within the constructed age model of core 41-2, different productivity proxies and magnetic records, combined with similar data from core 12KL (Max et al., 2012, 2014) reveal a sequence of noticeable centennial events of increased productivity in the NW Pacific which occurred in phase with Chinese sub-interstadials (CsI) associated with stronger EASM or weaker EAWM (Wang et al., 2008) and changes in atmospheric circulation during 21–8 ka (Figs. 3 and 4).

These linkages suggest that centennial increased productivity events in the NW Pacific were likely associated with shifts of a warmer regional climate and/or higher nutrient availability in surface water, synchronous with CsI of the EASM. According to Wang et al. (2001), the interstadials of EASM are broadly correlated with regional climate warming. High resolution records presented here show clearly that four centennial-scale events of increased productivity/environmental amelioration correlated with CsI during the LGM, four events during HE1, four events during the B/A warming, and four events during the EH (Fig. 4; Table 2).

4. Discussion

4.1 Productivity patterns during the LGM-HE 1

Besides the centennial productivity/environmental events, similar NW Pacific productivity patterns are found in cores 41-2 and 12KL during the LGM and HE1 with some differences in different productivity proxies. During the LGM, most proxies demonstrate a minimum primary productivity in the NW Pacific without definite trends (Fig. 4). Severe environmental conditions in central Asia inferred from pollen data (Bezrukova et al., 2010) (Fig. 5) seem to be promoted an increase in winter sea ice formation and sea ice cover in NW Pacific, consistent with high IRD accumulation inferred from CF and MS records (Fig. 4), that might have inhibited productivity in the study area. It is also consistent with the minimum productivity in the NW Pacific due to strong stratification, preventing the supply of nutrients required to support productivity in surface waters (Gebhardt et al., 2008).

From 17.8 to 15.3 ka, the TOC and chlorin contents associated with the production of calcareous phytoplankton (mostly coccolithophores) show a significant increase concurrently to the diminished AMOC (McManus et al., 2004). The diminished AMOC resulted in a major cooling of the Northern Hemisphere and, most likely, reduced water evaporation in the N Atlantic and therefore Atlantic-Pacific moisture transport. This condition facilitates an overall increase in surface

363 water salinity, and decrease in surface stratification in the N Pacific, promoting an intensified
364 ventilation of the intermediate water. The observed trends of productivity proxies are in concord
365 with strong intensification of the intermediate-depth water ventilation in the N Pacific during HE1
366 (Max et al., 2014). However, fairly constant $CaCO_3$ values in both cores (water depth 1924–2145
367 m) during the LGM-HE1 do not indicate that the water ventilation penetrated to deep water in the N
368 Pacific over that time interval, because carbonate concentration in the sediment is strongly
369 constrained by the ventilation of bathed water (Yu et al., 2013). The productivity proxies such as Si-
370 bio and color b*, associated with siliceous phytoplankton production (mostly diatoms), do not show
371 significant trends during HE1 up to ~15.3 ka. The enhanced coverage of sea ice, shown by CF and
372 MS records (Fig. 4), until 15.3 ka in the studied area probably lead to the overwhelmed production
373 of diatom, due to the subsequent large spring–early summer surface water stratification. Both CF
374 and MS records may represent IRD changes over the LGM-YD because the input of volcanic
375 materials estimated in CF was insignificant during 21-12 ka compared to that of the Holocene (Fig.
376 4).

377 A sharp increase in the NW Pacific primary production, and a rise in the diatom production
378 since ~15.3 ka indicated by most productivity proxies and Si-bio and color b* records with a peak at
379 sub-interstadial GI1-e of B/A warming (Fig. 4), was likely induced by a decreased effect of sea ice
380 and its spring melting, favoring a weakening of surface stratification. The timing of the decrease in
381 the sea ice cover since ~15.3 ka is consistent with the regional surface water warming (Max et al.,
382 2012). Such a pattern in productivity changes in the N Pacific and the Bering Sea during the
383 glacial/interglacial transitions has been reported in previous studies (Caissie et al., 2010; Galbraith
384 et al., 2007; Gebhardt et al., 2008; Gorbarenko, 1996; Keigwin, 1998) and was likely a persistent
385 feature of the N Pacific and its realm, forced by the resumption of the AMOC at the B/A warming.
386

387 ***4.2 Centennial variations in productivity during the LGM-HE1-B/A***

388 The identification of potential linkages between centennial climate changes in the Northern
389 Hemisphere (NW Pacific, EASM, and N Atlantic/Greenland) and the climate changes recorded in
390 the Antarctic ice cores is important for deepening our understanding of the mechanisms responsible
391 for the timing and spatial propagation patterns that resulted from abrupt variability in global climate
392 and environmental system. In order to test these linkages, the centennial productivity/climate events
393 in the NW Pacific outlined by the productivity stack are compared with records from the Northern
394 Hemisphere ($\delta^{18}O$ and Ca^{2+} of NGRIP, $\delta^{18}O$ of EASM, N Atlantic IRD, Siberian climate) and from
395 the Southern Hemisphere (Fig.5). It has been suggested that the nearly synchronous ice core $\delta^{18}O$
396 and Ca^{2+} millennial-scale changes reflect the shifting of the Greenland atmospheric dust loading,

which is closely linked with the atmospheric circulation and climate changes in the high latitudes of the Northern Hemisphere, where the EASM plays an important role (Ruth et al., 2007).

Similarity of glacial millennial-scale climate variability recorded in Chinese cave stalagmites and Greenland ice cores (Sun et al., 2012; Wang et al., 2001) implies a plausible influence of high-latitude climate of the Northern Hemisphere on the EASM by atmospheric circulation changes. Several main elements of atmospheric circulation, including the Intertropical Convergence Zone (ITCZ), northern westerly jet, AO and the SH, were previously considered as potential mechanisms linking abrupt climate changes in the N Atlantic and East Asia (Jin et al., 2007; Nagashima et al., 2011; Sung et al., 2006; Timmermann et al., 2007).

Apparent similarity of centennial climate and environment variability between the NW Pacific productivity events, EASM and Greenland records (Fig. 5) allow us to suggest that mechanisms responsible for their teleconnection were the same as on millennial scales. Remarkable similarity of sequence of the NW Pacific productivity events with the sub-interstadials of EASM records during the LGM-HE1 (Fig. 5) implies a strong common driver responded to their variations. Wu and Wang (2002) concluded that SH has provided direct and significant influence on the EAWM, particularly by sea level pressure and northerly wind along the East Asian Coast. Simultaneously, the SH strongly influences on the sea ice formation in the NW Pacific and marginal seas by the similar mechanisms like the wind intensity controlled by pressure gradient and winter air temperature at the sea level (Kimura and Wakatsuchi, 1999). Records of CF and MS, related with IRD accumulation, show that studied area off Kamchatka was undergone to the influence of sea ice during the LGM-HE1 (Fig. 4). Enhancement of SH, associated with abrupt climate cooling, led to an increase in terrigenous material delivery by sea ice from the coast and to a decrease in primary productivity by shrinking of productive season between events with increased productivity.

Correlation of the centennial changes in the NW Pacific productivity events / CsIs with Greenland sub interstadials during the LGM-HE1 was mainly observed but less clear, due to the discrepancy in constructed age models / or to whatever differences in atmospheric teleconnections (Fig. 5). There are some $\delta^{18}O$ differences between coeval $\delta^{18}O$ values in the Summit and NGRIP ice cores during the LGM-HE1, which were likely controlled by changes in the N American Ice Sheet volume and N Atlantic sea-ice coverage, resulting in the meridional discrepancy in the $\delta^{18}O$ of Greenland ice (Seierstad et al., 2014).

EPICA community members (2006) showed that methane synchronization of the EDML and the $\delta^{18}O$ of NGRIP reveal one-to-one alignment of each Antarctic warming with a corresponding stadial in the Greenland ice cores, implying a bipolar seesaw mechanism on millennial time scales.

Since it was shown that Chinese and Greenland interstadials have occurred synchronously (Wang et al., 2001), therefore, Chinese interstadials (CIs) were also, likely, related to the Antarctic cold events. For example, warmer conditions at the Antarctic during 23.6–24.3 ka (coeval with Chinese sub-stadial CsS-GS3-1) were synchronous with abrupt climate cooling and an increase in dust content in the Greenland ice cores NGRIP, coeval with HE2 of the N Atlantic, and in phase with the weakening of the EASM (GS/CS-3.1) (Fig.5). The Antarctic cooling after 23.4 ka was accompanied by warming in Greenland, with two sharp interstadials GI-2.2 and GI-2.1 (Rasmussen et al., 2014) and EASM interstadial CI-2 (Wang et al., 2001) (Fig. 5).

It has also been suggested that an index of monsoon intensity was controlled not only by the Northern Hemisphere temperature ("pull" on the monsoon, which is more intense during boreal warm periods), but also by the pole-to-equator temperature gradient in the Southern Hemisphere ("push" on the monsoon, which is more intense during the boreal cold periods) that leads to enhanced boreal summer monsoon intensity and its northward propagation (Rohling et al., 2009; Rossignol-Strick, 1985; Xue et al., 2004). Since EASM transports heat and moisture from the West Pacific Warm Pool (WPWP) to higher latitudes (Wang et al., 2001), the temperature gradient in the Southern Hemisphere "pushes" the northward propagation of EASM via the latitudinal/longitudinal migrations or expansion/contraction of the WPWP (Rohling et al., 2009; Xue et al., 2004). This also explains the difference in responses to the EASM and Greenland interstadials and sub-interstadials, because the migration of the WPWP may have occurred more slowly than the atmospheric circulation changes (Rohling et al., 2009; Xue et al., 2004). The changes in the $\delta^{18}O$ records of Chinese stalagmites were more gradual than in the $\delta^{18}O$ records of Greenland ice cores, and were more similar to the changes of Antarctic air temperature (Fig. 5). So, it is possible that forcing from low latitudes "push effect" on the EASM was additional mechanism in centennial productivity changes in the NW Pacific due to surface water amelioration. Although time resolution of the Antarctic $\delta^{18}O$ curve was not as high as ones from the Greenland and the EASM, records demonstrated in Figure 5 do not exclude one-to-one alignment of each Antarctic centennial cooling with related EASM sub-interstadial / NW Pacific productivity events.

We suggest that, in addition to the eight centennial productivity/environmental events during the LGM-HE1 established in the studied cores from the NW Pacific, other three abrupt productivity/climate events likely took place in the NW Pacific, synchronous with CsIs outlined by the $\delta^{18}O$ records of Chinese stalagmites and the Greenland during the interval of 25–20 ka (namely CsI-GS2.1-11, CsI-GS2.1-10, and CsI-GS2.1-9) (Fig. 5).

During the B/A warming and resumption of the AMOC, four sub-interstadials (CsI-GI1-a to CsI-GI1-e) were clearly and simultaneously observed in the Greenland ice cores $\delta^{18}O$ (Björck et al.,

1998) and dust records and EASM sub-interstadials synchronously with centennial productivity / environment events of the NW Pacific (Fig. 5). It is consistent with enhancement of the "pull effect" on the intensified EASM and therefore amelioration of the NW Pacific during boreal warm period, which implies a dominant control of Northern Hemisphere climate processes on the atmospheric circulation in high latitudes (Rohling et al., 2009). Related significant coeval changes in the atmosphere circulation with periodicity *ca* 0.4 ka exert strong influence on the climate and environment in ocean and continent of the Northern Hemisphere during the B/A (Bezrukova et al., 2010).

4.3 Centennial variations in productivity during the EH

During the EH the records presented here show an alternation of the four NW Pacific centennial events with lower and four ones with higher productivity, namely as CsS-EH-1 -CsS-EH-4 and CsI-EH-1 - CsI-EH-4, respectively (Figs. 4 and 5; Table 2). The low productivity events (CsS-EH-1 and CsS-EH-2) are likely correlated with Greenland cold events at 8.2 ka and 9.3 ka, respectively (Rasmussen et al., 2014). Also, the NW Pacific low productivity events (CsS-EH-1, CsS-EH-2 and CsS-EH-3) occurred synchronously with the EASM decrease and whatever climate cooling recorded in $\delta^{18}O$ of the Dongge cave stalagmite D4 (Dykoski et al., 2005) (Fig. 5). Therefore it may be suggested that during the EH the NW Pacific events with higher / lower productivity had occurred coeval with climate warming / cooling as well. The pollen-based reconstruction of the variability of the vegetation / climate from a well-dated core from south Siberia (Lake Baikal region) (Bezrukova et al., 2010) demonstrated nearly the same pattern of centennial variability during the EH (Fig. 5). Well-dated, high resolution lithological and geochemical results from the Yanchi playa (NE China) also clearly showed a sequence of three sharp cooling events at 8.2 ka, 9.9–10.1 ka, and 11.0–11.2 ka (Yu et al., 2006), quasi-synchronous with the NW Pacific productivity / climate events CsS-EH-1, CsS-EH-3 and CsS-EH-4. Yu et al. (2006) explained this correlation through linkages between the tropical Pacific and N Atlantic.

An alternation of the NW Pacific events with lower / higher productivity during the EH demonstrates a perfect correlation with periodicities of solar activity and the production of the cosmogenic nuclides ^{14}C and ^{10}Be (Reimer et al., 2004) (Fig. 5). The production rates of these cosmogenic nuclides and residual atmospheric $\Delta^{14}C$ record are negatively correlated with total solar irradiance due to the strength of magnetic fields embedded into the solar wind (Hu et al., 2003). Small variations in solar irradiance could be responsible for pronounced changes in northern high-latitude climate and environments (Bond et al., 2001; Hu et al., 2003). The NW Pacific events of higher productivity occurred during increased solar irradiance and climate warming, indicating that variability of the solar irradiance was a potential driver of the climate and environmental changes in

498 the NW Pacific during the EH. The low productivity / cold climate CsS-EH-2 event in records of
499 atmospheric $\Delta^{14}C$ and the Greenland $\delta^{18}O$ ice core was marked by sharp cooling at its onset and
500 termination with some warming during the transition (Fig. 5). The CsS-EH-4 event shows a similar
501 pattern in records of productivity stack and $\delta^{18}O$ of the Greenland and Dongge cave D4, indicating
502 fine structure of these cold events.

503 The influence of variations in solar output on hydrography of surface ocean in the subpolar
504 N Atlantic during the Holocene was reported by Bond et al. (2001). The variability of subpolar N
505 Atlantic ice drifting, recorded as the percentage of hematite-stained grains (Bond et al., 2001),
506 though having lower time resolution and dating precision compared with production of the
507 cosmogenic nuclides, is consistent with other centennial climate changes in the Northern
508 Hemisphere during the EH (Fig. 5).

509 The high resolution records of an alternation of the NW Pacific events with lower / higher
510 productivity related with climate cooling / warming, demonstrating that centennial scale climate
511 events during the EH were similar between the N Atlantic and NW Pacific, possibly because of the
512 close linkages of sun-ocean-climate, consistent with earlier conclusions (Bond et al., 2001; Hong et
513 al., 2009; Hu et al., 2003).

514 ***4.4 Cross-correlation of the N Atlantic-NW Pacific climate variability***

515 Since whether N Atlantic-NW Pacific climate and hydrological in-phase or out-of-phase
516 linkages are still under debate, empirical data obtained from sediment cores off Kamchatka offer the
517 provision for clarifying this issue at high resolution. Here we provide comparison of the
518 productivity stack of core 41-2, responsible for NW Pacific environmental variability, and $\delta^{18}O$
519 records of the NGRIP ice core, responsible for the Greenland / N Atlantic climate changes
520 (Rasmussen et al., 2014). Cross correlation of these records using moving windows at 2000 years
521 shows more significant synchronization (from -0.6 to - 0.9) from 15.8 ka up to 10.8 ka confirming
522 strong atmospheric teleconnections between the NW Pacific and the N Atlantic during this period
523 (Fig. 6). Cross correlation during early (19 ka - 15.8 ka) and later periods (10.8 ka - 9 ka) indicates
524 weak NW Pacific - N Atlantic linkages, but do not support the out-of-phased hypothesis.

525

526 **5. Conclusions**

527 This study presents high resolution records of productivity proxies (TOC, $CaCO_3$, chlorin,
528 color b*, Ba-bio, Br-bio and Si-bio), sediment lithological, and magnetic properties from sediment
529 cores, 41-2 and 12KL, taken from the NW Pacific. Results presented here reveal 16 centennial
530 regional productivity events during the LGM-EH (20–8 ka) in the NW Pacific. Four NW Pacific
531 abrupt productivity increased events are linked to CsIs during the LGM (20–17.8 ka), four ones

during HE 1 (17.8–14.7 ka) and four ones during the B/A. An alternative occurrence of four centennial events with lower and higher productivity was established during the EH.

On the basis of age models of cores 41-2 and 12KL, we suggest that NW Pacific centennial events of increased productivity occur synchronously with sub-interstadials of the EASM. These NW Pacific events and EASM sub-interstadials are positively correlated with Greenland abrupt warming, indicating an atmospheric teleconnection between the NW Pacific and the N Atlantic during the LGM-HE 1-B/A.

Remarkable similarity of the sequence of productivity events recorded in the NW Pacific with the EASM sub-interstadials during the LGM-HE1 implies that SH is a strong driver responded to their variation. The comparison between our stacked productivity with the $\delta^{18}O$ of the EPICA, NGRIP and EASM suggest that another mechanism associated with temperature gradient in the Southern Hemisphere ("pushes effect") may be responded to the EASM sub-interstadials and subsequent variability in productivity events in the NW Pacific on centennial time scale during the LGM-HE1.

During the B/A warming and resumption of the AMOC, synchronicity between the productivity events, EASM sub-interstadials, and the $\delta^{18}O$ and dust records in the NGRIP is consistent with enhancement of the "pull effect" on the monsoon's intensity, which implies a dominant control of atmospheric processes on the productivity and climate of the NW Pacific.

During the EH, the high resolution records of an alternation of productivity events with lower / higher productivity related with climate cooling / warming, reveal that centennial climate events were similar between the subpolar regions of the N Atlantic and NW Pacific, and were controlled by mechanisms of sun-ocean-climate linkages.

In summary, the NW Pacific results presented here indicate a tight linkage and coherent pattern of centennial - millennial scale climate changes during the LGM-EH, which may serve as a template in high resolution paleoceanography and sediment stratigraphy of the moderate-high latitudes in the NW Pacific.

Acknowledgements

We are grateful to Drs. Ralf Tiedemann and Dirk Nürnberg (AWI, GEOMAR, Germany) for a long and fruitful cooperation, and for providing samples and the dataset of core 12KL. We are indebted to Dr. John Southon (USA) for the AMS ^{14}C dating. We thank Dr. Selvaraj Kandasamy (Xiamen University) to correct the paper. This research work was supported by the RFBR (Russian Fund of Basic Research), Russian project (13-05-00296a, 16-55-53048 and 16-05-00127), Russian Federation budget (No 01201363042), the International Cooperation Project of Global Change and Ocean-Atmosphere Interaction (GASIGEOGE-04), National Natural Science Foundation of China

(Grant Nos.: 41476056, 41611130042 and U1606401) and by International Cooperative Projects in polar regions (201613), and the Russia-Taiwan Research Cooperation projects (14-HHC-002 and 17-MHT-003).

References

Barron, J. A., Heusser, L., Herbert, T. and Lyle, M.: High-resolution climatic evolution of coastal northern California during the past 16,000 years, Paleoceanography, 18(1), doi:10.1029/2002PA000768, 2003.

Barron, J. A., Bukry, D., Dean, W. E., Addison, J. A. and Finney, B.: Paleoceanography of the Gulf of Alaska during the past 15,000 years: Results from diatoms, silicoflagellates, and geochemistry, Mar. Micropaleontol., 72(3–4), 176–195, doi:10.1016/j.marmicro.2009.04.006, 2009.

Berger, W. H., Smetacek, V. S. and Wefer, G.: Ocean Productivity and Paleoproductivity - An Overview, in Productivity of the Ocean: Present and Past, pp. 1–34., 1989.

Bezrukova, E. V., Tarasov, P. E., Solovieva, N., Krivonogov, S. K. and Riedel, F.: Last glacial–interglacial vegetation and environmental dynamics in southern Siberia: Chronology, forcing and feedbacks, Palaeogeogr. Palaeoclimatol. Palaeoecol., 296(1–2), 185–198, doi:10.1016/j.palaeo.2010.07.020, 2010.

Björck, S., Walker, M. J. C., Cwynar, L. C., Johnsen, S., Knudsen, K.-L., Lowe, J. J. and Wohlfarth, B.: An event stratigraphy for the Last Termination in the North Atlantic region based on the Greenland ice-core record: a proposal by the INTIMATE group, J. Quat. Sci., 13(4), 283–292, doi:10.1002/(SICI)1099-1417(199807/08)13:4<283::AID-JQS386>3.0.CO;2-A, 1998.

Bond, G. C., Kromer, B., Beer, J., Muscheler, R., Evans, M. N., Showers, W., Hoffmann, S., Lotti-Bond, R., Hajdas, I. and Bonani, G.: Persistent solar influence on North Atlantic climate during the Holocene, Science, 294(5549), 2130–6, doi:10.1126/science.1065680, 2001.

Caissie, B. E., Brigham-Grette, J., Lawrence, K. T., Herbert, T. D. and Cook, M. S.: Last Glacial Maximum to Holocene sea surface conditions at Umnak Plateau, Bering Sea, as inferred from diatom, alkenone, and stable isotope records, Paleoceanography, 25(1), PA1206, doi:10.1029/2008PA001671, 2010.

Channell, J. E. T., Xuan, C. and Hodell, D. A.: Stacking paleointensity and oxygen isotope data for the last 1.5 Myr (PISO-1500), Earth Planet. Sci. Lett., 283(1–4), 14–23, doi:10.1016/j.epsl.2009.03.012, 2009.

Chikamoto, M. O., Menviel, L., Abe-Ouchi, A., Ohgaito, R., Timmermann, A., Okazaki, Y.,

598 Harada, N., Oka, A. and Mouchet, A.: Variability in North Pacific intermediate and deep water
599 ventilation during Heinrich events in two coupled climate models, Deep Sea Res. Part II Top. Stud.
600 Oceanogr., 61–64, 114–126, doi:10.1016/j.dsr2.2011.12.002, 2012.

601 Dansgaard, W., Johnsen, S. J., Clausen, H. B., Dahl-Jensen, D., Gundestrup, N. S., Hammer, C. U.,
602 Hvidberg, C. S., Steffensen, J. P., Sveinbjörn, Jouzel, J. and Bond, G. C.: Evidence for general
603 instability of past climate from a 250-kyr ice-core record, Nature, 364(6434), 218–220,
604 doi:10.1038/364218a0, 1993.

605 Dykoski, C. A., Edwards, R. L., Cheng, H., Yuan, D., Cai, Y., Zhang, M., Lin, Y., Qing, J., An, Z.
606 and Revenaugh, J.: A high-resolution, absolute-dated Holocene and deglacial Asian monsoon
607 record from Dongge Cave, China, Earth Planet. Sci. Lett., 233(1–2), 71–86,
608 doi:10.1016/j.epsl.2005.01.036, 2005.

609 Dymond, J., Suess, E. and Lyle, M.: Barium in Deep-Sea Sediment: A Geochemical Proxy for
610 Paleoproductivity, Paleoceanography, 7(2), 163–181, doi:10.1029/92PA00181, 1992.

611 Enkin, R. J., Baker, J., Nourgaliev, D., Iassonov, P. and Hamilton, T. S.: Magnetic hysteresis
612 parameters and Day plot analysis to characterize diagenetic alteration in gas hydrate-bearing
613 sediments, J. Geophys. Res., 112(B06S90), 1–13, doi:10.1029/2006JB004638, 2007.

614 EPICA Community Members: One-to-one coupling of glacial climate variability in Greenland and
615 Antarctica, Nature, 444(7116), 195–198, doi:10.1038/nature05301, 2006.

616 Favorite, F., Dodimead, A. J. and Nasu, K.: Oceanography of the Subarctic Pacific region, 1960-
617 1971., 1976.

618 Fletcher, W. J., Sanchez Goñi, M. F., Allen, J. R. M., Cheddadi, R., Combourieu-Nebout, N.,
619 Huntley, B., Lawson, I., Londeix, L., Magri, D., Margari, V., Müller, U. C., Naughton, F.,
620 Novenko, E., Roucoux, K. and Tzedakis, P. C.: Millennial-scale variability during the last glacial in
621 vegetation records from Europe, Quat. Sci. Rev., 29(21–22), 2839–2864,
622 doi:10.1016/j.quascirev.2009.11.015, 2010.

623 Galbraith, E. D., Jaccard, S. L., Pedersen, T. F., Sigman, D. M., Haug, G. H., Cook, M., Southon, J.
624 R. and Francois, R.: Carbon dioxide release from the North Pacific abyss during the last
625 deglaciation., Nature, 449(7164), 890–893, doi:10.1038/nature06227, 2007.

626 Gebhardt, H., Sarnthein, M., Grootes, P. M., Kiefer, T., Kuehn, H., Schmieder, F. and Röhl, U.:
627 Paleonutrient and productivity records from the subarctic North Pacific for Pleistocene glacial
628 terminations I to V, Paleoceanography, 23(4), doi:10.1029/2007PA001513, 2008.

Goldberg, E. D. and Arrhenius, G. O. S.: Chemistry of Pacific pelagic sediments, Geochim. Cosmochim. Acta, 13(2–3), 153–212, doi:10.1016/0016-7037(58)90046-2, 1958.

Goldberg, E. L. E. L., Gorbarenko, S. A. S. A., Shaporenko, A. D., Bosin, A. A. A. A., Leskov, V. Y. Y. and Chebykin, E. P. P.: Instability of last glacial climate from SRXFA data for bottom sediments in the Okhotsk Sea, Nucl. Instruments Methods Phys. Res. Sect. A Accel. Spectrometers, Detect. Assoc. Equip., 543(1), 284–287, doi:10.1016/j.nima.2005.01.242, 2005.

Gorbarenko, S. A.: Stable Isotope and Lithologic Evidence of Late-Glacial and Holocene Oceanography of the Northwestern Pacific and Its Marginal Seas, Quat. Res., 46(3), 230–250, doi:10.1006/qres.1996.0063, 1996.

Gorbarenko, S. A. and Goldberg, E. L.: Assessment of Variations of Primary Production in the Sea of Okhotsk, Bering Sea, and Northwestern Pacific over the Last Glaciation Maximum and Holocene, Dokl. Earth Sci., 405(9), 1380–1383, 2005.

Gorbarenko, S. A., Chekhovskaya, M. P. and Southon, J. R.: Detailed environmental changes of the Okhotsk Sea central part during last Glaciation Holocene, Oceanologia, 38(2), 305–308, 1998.

Gorbarenko, S. A., Leskov, V. Y., Artemova, A. V., Tiedemann, R., Biebow, N. and Nürnberg, D.: Ice Cover of the Sea of Okhotsk during the Last Glaciation and Holocene, Dokl. Earth Sci., 389(2), 208–211, 2003.

Gorbarenko, S. A., Southon, J. R. J. ., Keigwin, L. D., Cherepanova, M. . and Gvozdeva, I. . G.: Late Pleistocene–Holocene oceanographic variability in the Okhotsk Sea: geochemical, lithological and paleontological evidence, Palaeogeogr. Palaeoclimatol. Palaeoecol., 209(1–4), 281–301, doi:10.1016/j.palaeo.2004.02.013, 2004.

Gorbarenko, S. A., Basov, I. A., Chekhovskaya, M. P. P., Southon, J. R., Khusid, T. A. A. and Artemova, A. V.: Orbital and millennium scale environmental changes in the southern Bering Sea during the last glacial-Holocene: Geochemical and paleontological evidence, Deep Sea Res. Part II Top. Stud. Oceanogr., 52(16–18), 2174–2185, doi:10.1016/j.dsr2.2005.08.005, 2005.

Gorbarenko, S. A. S. A., Harada, N., Malakhov, M. I. M. I., Velivetskaya, T. A. T. A., Vasilenko, Y. P. Y. P., Bosin, A. A. A. A., Derkachev, A. N. A. N., Goldberg, E. L. E. L. and Ignatiev, A. V. A. V.: Responses of the Okhotsk Sea environment and sedimentology to global climate changes at the orbital and millennial scale during the last 350kyr, Deep Sea Res. Part II Top. Stud. Oceanogr., 61–64, 73–84, doi:10.1016/j.dsr2.2011.05.016, 2012.

Harada, N.: MIRAI cruise report MR06-04 Leg 1 and 2, JAMSTEC, Yokosuka. [Available at http://www.godac.jamstec.go.jp/cruisedata/mirai/e/MR06-04_leg1.html]., 2006.

Harada, N., Sato, M. and Sakamoto, T.: Freshwater impacts recorded in tetraunsaturated alkenones and alkenone sea surface temperatures from the Okhotsk Sea across millennial-scale cycles, Paleoceanography, 23(3), doi:10.1029/2006PA001410, 2008.

Harris, P. G., Zhao, M., Rosell-Melé, A., Tiedemann, R., Sarnthein, M. and Maxwell, J. R.: Chlorin accumulation rate as a proxy for Quaternary marine primary productivity, Nature, 383(6595), 63–65, doi:10.1038/383063a0, 1996.

Hong, Y. T., Hong, B., Lin, Q. H., Shibata, Y., Zhu, Y. X., Leng, X. T. and Wang, Y.: Synchronous climate anomalies in the western North Pacific and North Atlantic regions during the last 14,000 years, Quat. Sci. Rev., 28(9–10), 840–849, doi:10.1016/j.quascirev.2008.11.011, 2009.

Hu, F. S., Kaufman, D., Yoneji, S., Nelson, D., Shemesh, A., Huang, Y., Tian, J., Bond, G. C., Clegg, B. and Brown, T. A.: Cyclic variation and solar forcing of Holocene climate in the Alaskan subarctic., Science, 301(5641), 1890–1893, doi:10.1126/science.1088568, 2003.

Jaccard, S. L., Galbraith, E. D., Sigman, D. M. and Haug, G. H.: A pervasive link between Antarctic ice core and subarctic Pacific sediment records over the past 800 kyrs, Quat. Sci. Rev., 29(1–2), 206–212, doi:10.1016/j.quascirev.2009.10.007, 2010.

Jasonov, P. G., Nurgaliev, D. K., Burov, B. V. and Heller, F.: A modernized coercivity spectrometer, Geol. Carpathica, 49(3), 2254–225, 1998.

Jin, L., Chen, F., Ganopolski, A. and Claussen, M.: Response of East Asian climate to Dansgaard/Oeschger and Heinrich events in a coupled model of intermediate complexity, J. Geophys. Res., 112(D6), D06117, doi:10.1029/2006JD007316, 2007.

Johnsen, S. J., Clausen, H. B., Dansgaard, W., Fuhrer, K., Gundestrup, N., Hammer, C. U., Iversen, P., Jouzel, J., Stauffer, B. and Steffensen, J. P.: Irregular glacial interstadials recorded in a new Greenland ice core, Nature, 359(6393), 311–313, doi:10.1038/359311a0, 1992.

Keigwin, L. D.: Glacial-age hydrography of the far northwest Pacific Ocean, Paleoceanography, 13(4), 323–339, doi:10.1029/98PA00874, 1998.

Keigwin, L. D., Jones, G. A. and Froelich, P. N.: A 15,000 year paleoenvironmental record from Meiji Seamount, far northwestern Pacific, Earth Planet. Sci. Lett., 111(2–4), 425–440, doi:10.1016/0012-821X(92)90194-Z, 1992.

Kennett, J. P., Roark, E. B., Cannariato, K. G., Ingram, B. L. and Tada, R.: Latest quaternary paleoclimatic and radiocarbon chronology, Hole 1017E, Southern California margin, Proc. Ocean Drill. Progr., 167, 249–254, 2000.

692 Kiefer, T., Sarnthein, M., Erlenkeuser, H., Grootes, P. M. and Roberts, A. P.: North Pacific
693 response to millennial-scale changes in ocean circulation over the last 60 kyr, Paleoceanography,
694 16(2), 179–189, doi:10.1029/2000PA000545, 2001.

695 Kienast, S. S. and McKay, J. L.: Sea surface temperature in the subartic Northeast Pacific reflect
696 millennial-scale climate oscillations during the last 16 kyr, Geophys. Res. Lett., 28(8), 1563–1566,
697 2001.

698 Kim, S.-J., Khim, B.-K., Uchida, M., Itaki, T. and Tada, R.: Millennial-scale paleoceanographic
699 events and implication for the intermediate-water ventilation in the northern slope area of the
700 Bering Sea during the last 71 kyrs, Glob. Planet. Change, 79(1–2), 89–98,
701 doi:10.1016/j.gloplacha.2011.08.004, 2011.

702 Kimura, N. and Wakatsuchi, M.: Processes controlling the advance and retreat of sea ice in the Sea
703 of Okhotsk, J. Geophys. Res., 104(C5), 11137, doi:10.1029/1999JC900004, 1999.

704 Lisitzin, A. P.: Sea-Ice and Iceberg Sedimentation in the Ocean, Springer, Berlin, Heidelberg.,
705 2002.

706 Malakhov, M. I. M. I., Gorbarenko, S. A. S. A., Malakhova, G. Y., Harada, N., Vasilenko, Y. P.,
707 Bosin, A. A. A. A., Gol'dberg, E. L., Derkachev, A. N. A. N., Goldberg, E. L. and Derkachev, A.
708 N. A. N.: Petromagnetic parameters of bottom sediments as indicators of the climatic and
709 environmental changes in the central zone of the Sea of Okhotsk during the last 350 kyr, Russ.
710 Geol. Geophys., 50(11), 973–982, doi:10.1016/j.rgg.2009.10.006, 2009.

711 Max, L., Riethdorf, J.-R., Tiedemann, R., Smirnova, M., Lembke-Jene, L., Fahl, K., Nürnberg, D.,
712 Matul, A. G. and Mollenhauer, G.: Sea surface temperature variability and sea-ice extent in the
713 subarctic northwest Pacific during the past 15,000 years, Paleoceanography, 27(3),
714 doi:10.1029/2012PA002292, 2012.

715 Max, L., Lembke-Jene, L., Riethdorf, J.-R., Tiedemann, R., Nürnberg, D., Kühn, H. and
716 Mackensen, A.: Pulses of enhanced North Pacific Intermediate Water ventilation from the Okhotsk
717 Sea and Bering Sea during the last deglaciation, Clim. Past, 10(2), 591–605, doi:10.5194/cp-10-
718 591-2014, 2014.

719 McManus, J., Berelson, W. M., Klinkhammer, G. P., Johnson, K. S., Coale, K. H., Anderson, R. F.,
720 Kumar, N., Burdige, D. J., Hammond, D. E., Brumsack, H. J., McCorkle, D. C. and Rushdi, A.:
721 Geochemistry of barium in marine sediments: implications for its use as a paleoproxy, Geochim.
722 Cosmochim. Acta, 62(21–22), 3453–3473, doi:10.1016/S0016-7037(98)00248-8, 1998.

723 McManus, J. F., Francois, R., Gherardi, J.-M., Keigwin, L. D. and Brown-Leger, S.: Collapse and

724 rapid resumption of Atlantic meridional circulation linked to deglacial climate changes., Nature,
725 428(6985), 834–837, doi:10.1038/nature02494, 2004.

726 Nagashima, K., Tada, R., Tani, A., Sun, Y., Isozaki, Y., Toyoda, S. and Hasegawa, H.: Millennial-
727 scale oscillations of the westerly jet path during the last glacial period, J. Asian Earth Sci., 40(6),
728 1214–1220, doi:10.1016/j.jseaes.2010.08.010, 2011.

729 Narita, H., Sato, M., Tsunogai, S., Murayama, M., Ikehara, M., Nakatsuka, T., Wakatsuchi, M.,
730 Harada, N. and Ujiié, Y.: Biogenic opal indicating less productive northwestern North Pacific
731 during the glacial ages, Geophys. Res. Lett., 29(15), 22-1-22–4, doi:10.1029/2001GL014320, 2002.

732 Nilsson, T.: The Pleistocene; Geology and Life in the Quaternary Ice Age, D. Reidel, Dordrecht.,
733 1983.

734 North Greenland Ice Core Project members: High-resolution record of Northern Hemisphere
735 climate extending into the last interglacial period, Nature, 431(7005), 147–151,
736 doi:10.1038/nature02805, 2004.

737 Nürnberg, D. and Tiedemann, R.: Environmental change in the Sea of Okhotsk during the last 1.1
738 million years, Paleoceanography, 19(4), PA4011, doi:10.1029/2004PA001023, 2004.

739 Okazaki, Y., Timmermann, A., Menviel, L., Harada, N., Abe-Ouchi, A., Chikamoto, M. O.,
740 Mouchet, A. and Asahi, H.: Deepwater formation in the North Pacific during the Last Glacial
741 Termination., Science, 329(5988), 200–204, doi:10.1126/science.1190612, 2010.

742 Praetorius, S. K. and Mix, A. C.: Synchronization of North Pacific and Greenland climates preceded
743 abrupt deglacial warming, Science, 345(6195), 444–448, doi:10.1126/science.1252000, 2014.

744 Prahl, F. G., Muehlhausen, L. A. and Lyle, M.: An organic geochemical assessment of
745 oceanographic conditions at Manop Site C over the past 26,000 years, Paleoceanography, 4(5),
746 495–510, doi:10.1029/PA004i005p00495, 1989.

747 Rasmussen, S. O., Bigler, M., Blockley, S. P., Blunier, T., Buchardt, S. L., Clausen, H. B.,
748 Cvijanovic, I., Dahl-Jensen, D., Johnsen, S. J., Fischer, H., Gkinis, V., Guillevic, M., Hoek, W. Z.,
749 Lowe, J. J., Pedro, J. B., Popp, T., Seierstad, I. K., Steffensen, J. P., Svensson, A. M., Vallelonga,
750 P., Vinther, B. M., Walker, M. J. C., Wheatley, J. J. and Winstrup, M.: A stratigraphic framework
751 for abrupt climatic changes during the Last Glacial period based on three synchronized Greenland
752 ice-core records: refining and extending the INTIMATE event stratigraphy, Quat. Sci. Rev., 106,
753 14–28, doi:10.1016/j.quascirev.2014.09.007, 2014.

754 Reimer, P. J., Baillie, M. G. L., Bard, E., Beck, J. W., Bertrand, C. J. H., Blackwell, P. G., Buck, C.

E., Burr, G. S., Cutler, K. B., Damon, P. E., Edwards, R. L., Fairbanks, R. G., Friedrich, M. and Guilderson, T. P.: IntCal04 terrestrial radiocarbon age calibration, 0–26 cal kyr BP, Radiocarbon, 46(3), 1029–1058, 2004.

Reimer, P. J., Bard, E., Bayliss, A., Beck, J. W., Blackwell, P. G., Bronk Ramsey, C., Buck, C. E., Cheng, H., Edwards, R. L., Friedrich, M., Grootes, P. M., Guilderson, T. P., Haflidason, H., Hajdas, I., Hatte, C., Heaton, T. J., Hoffmann, D. L., Hogg, A. G., Hughen, K. A., Kaiser, K. F., Kromer, B., Manning, S. W., Niu, M., Reimer, R. W., Richards, D. A., Scott, E. M., Southon, J. R., Staff, R. A., Turney, C. S. M. and van der Plicht, J.: IntCal13 and Marine13 Radiocarbon Age Calibration Curves 0–50,000 Years cal BP, Radiocarbon, 55(4), 1869–1887, doi:10.2458/azu_js_rc.55.16947, 2013.

Riethdorf, J.-R., Nürnberg, D., Max, L., Tiedemann, R., Gorbarenko, S. A. and Malakhov, M. I.: Millennial-scale variability of marine productivity and terrigenous matter supply in the western Bering Sea over the past 180 kyr, Clim. Past, 9(3), 1345–1373, doi:10.5194/cp-9-1345-2013, 2013.

Riethdorf, J.-R., Thibodeau, B., Ikehara, M., Nürnberg, D., Max, L., Tiedemann, R., Yokoyama, Y., Riethdorf, J.-R., Thibodeau, B., Ikehara, M., Nürnberg, D., Max, L., Tiedemann, R. and Yokoyama, Y.: Surface nitrate utilization in the Bering sea since 180kA BP: Insight from sedimentary nitrogen isotopes, Deep Sea Res. Part II Top. Stud. Oceanogr., 125–126, 163–176, doi:10.1016/j.dsr2.2015.03.007, 2016.

Röhl, U. and Abrams, L. J.: High-resolution, downhole, and nondestructive core measurements from Sites 999 and 1001 in the Caribbean Sea: application to the Late Paleocene Thermal Maximum, in Proceedings of the Ocean Drilling Program, 165 Scientific Results, vol. 165, pp. 191–203, Ocean Drilling Program., 2000.

Rohling, E. J., Liu, Q. S., Roberts, a. P., Stanford, J. D., Rasmussen, S. O., Langen, P. L. and Siddall, M.: Controls on the East Asian monsoon during the last glacial cycle, based on comparison between Hulu Cave and polar ice-core records, Quat. Sci. Rev., 28, 3291–3302, doi:10.1016/j.quascirev.2009.09.007, 2009.

Rossignol-Strick, M.: Mediterranean Quaternary sapropels, an immediate response of the African monsoon to variation of insolation, Palaeogeogr. Palaeoclimatol. Palaeoecol., 49(3–4), 237–263, doi:10.1016/0031-0182(85)90056-2, 1985.

Rothwell, R. G.: The Smear Slide Method, in Minerals and Mineraloids in Marine Sediments, pp. 21–24, Springer Netherlands, Dordrecht., 1989.

Ruth, U., Bigler, M., Röthlisberger, R., Siggaard-Andersen, M.-L., Kipfstuhl, S., Goto-Azuma, K.,

787 Hansson, M. E., Johnsen, S. J., Lu, H. and Steffensen, J. P.: Ice core evidence for a very tight link
788 between North Atlantic and east Asian glacial climate, Geophys. Res. Lett., 34(L03706), 1–5,
789 doi:10.1029/2006GL027876, 2007.

790 Sakamoto, T., Ikehara, M., Aoki, K., Iijima, K., Kimura, N., Nakatsuka, T. and Wakatsuchi, M.:
791 Ice-rafted debris (IRD)-based sea-ice expansion events during the past 100 kyrs in the Okhotsk Sea,
792 Deep Sea Res. Part II Top. Stud. Oceanogr., 52(16–18), 2275–2301,
793 doi:10.1016/j.dsr2.2005.08.007, 2005.

794 Sarnthein, M., Kiefer, T., Grootes, P. M., Elderfield, H. and Erlenkeuser, H.: Warmings in the far
795 northwestern Pacific promoted pre-Clovis immigration to America during Heinrich event 1,
796 Geology, 34(3), 141–144, doi:10.1130/G22200.1, 2006.

797 Schlung, S. A., Christina Ravelo, A., Aiello, I. W., Andreasen, D. H., Cook, M. S., Drake, M.,
798 Dyez, K. A., Guilderson, T. P., LaRiviere, J. P., Stroynowski, Z. and Takahashi, K.: Millennial-
799 scale climate change and intermediate water circulation in the Bering Sea from 90 ka: A high-
800 resolution record from IODP Site U1340, Paleoceanography, 28(1), 54–67,
801 doi:10.1029/2012PA002365, 2013.

802 Seierstad, I. K., Abbott, P. M., Bigler, M., Blunier, T., Bourne, A. J., Brook, E. J., Buchardt, S. L.,
803 Buizert, C., Clausen, H. B., Cook, E., Dahl-Jensen, D., Davies, S. M., Guillevic, M., Johnsen, S. J.,
804 Pedersen, D. S., Popp, T. J., Rasmussen, S. O., Severinghaus, J. P., Svensson, A. and Vinther, B.
805 M.: Consistently dated records from the Greenland GRIP, GISP2 and NGRIP ice cores for the past
806 104 ka reveal regional millennial-scale δ18O gradients with possible Heinrich event imprint, Quat.
807 Sci. Rev., 106, 29–46, doi:10.1016/j.quascirev.2014.10.032, 2014.

808 Seki, O., Ishiwatari, R. and Matsumoto, K.: Millennial climate oscillations in NE Pacific surface
809 waters over the last 82 kyr: New evidence from alkenones, Geophys. Res. Lett., 29(23), 59-1-59–4,
810 doi:10.1029/2002GL015200, 2002.

811 Seki, O., Ikehara, M., Kawamura, K., Nakatsuka, T., Ohnishi, K., Wakatsuchi, M., Narita, H. and
812 Sakamoto, T.: Reconstruction of paleoproductivity in the Sea of Okhotsk over the last 30 kyr,
813 Paleoceanography, 19(1), doi:10.1029/2002PA000808, 2004.

814 Serno, S., Winckler, G., Anderson, R. F., Maier, E., Ren, H., Gersonde, R. and Haug, G. H.:
815 Comparing dust flux records from the Subarctic North Pacific and Greenland: Implications for
816 atmospheric transport to Greenland and for the application of dust as a chronostratigraphic tool,
817 Paleoceanography, 30(6), 583–600, doi:10.1002/2014PA002748, 2015.

818 Siddall, M., Kaplan, M. R., Schaefer, J. M., Putnam, A., Kelly, M. A. and Goehring, B.: Changing

influence of Antarctic and Greenlandic temperature records on sea-level over the last glacial cycle, Quat. Sci. Rev., 29(3–4), 410–423, doi:10.1016/j.quascirev.2009.11.007, 2010.

Stuiver, M. and Reimer, P. J.: Extended 14C Data Base and Revised Calib 3.0 14C Age Calibration Program, Radiocarbon, 35(1), 215–230, 1993.

Stuiver, M., Grootes, P. M. and Braziunas, T. F.: The GISP2 δ18O Climate Record of the Past 16,500 Years and the Role of the Sun, Ocean, and Volcanoes, Quat. Res., 44(3), 341–354, doi:10.1006/qres.1995.1079, 1995.

Sun, Y., Clemens, S. C., Morrill, C., Lin, X., Wang, X. and An, Z.: Influence of Atlantic meridional overturning circulation on the East Asian winter monsoon, Nat. Geosci., 5(1), 46–49, doi:10.1038/ngeo1326, 2012.

Sung, M.-K., Kwon, W.-T., Baek, H.-J., Boo, K.-O., Lim, G.-H. and Kug, J.-S.: A possible impact of the North Atlantic Oscillation on the east Asian summer monsoon precipitation, Geophys. Res. Lett., 33(21), L21713, doi:10.1029/2006GL027253, 2006.

Tarasov, P. E., Bezrukova, E. V. and Krivonogov, S. K.: Late Glacial and Holocene changes in vegetation cover and climate in southern Siberia derived from a 15 kyr long pollen record from Lake Kotokel, Clim. Past, 5(3), 285–295, doi:10.5194/cp-5-285-2009, 2009.

Tauxe, L.: Sedimentary records of relative paleointenstiy of the geomagnetic field: theory and practice, Rev. Geophys., 31(93), 319–354, 1993.

Timmermann, A., Lorenz, S. J., An, S.-I., Clement, A. and Xie, S.-P.: The Effect of Orbital Forcing on the Mean Climate and Variability of the Tropical Pacific, J. Clim., 20(16), 4147–4159, doi:10.1175/JCLI4240.1, 2007.

Walker, M. J. C., Berkelhammer, M., Björck, S., Cwynar, L. C., Fisher, D. A., Long, A. J., Lowe, J. J., Newnham, R. M., Rasmussen, S. O. and Weiss, H.: Formal subdivision of the Holocene Series/Epoch: a Discussion Paper by a Working Group of INTIMATE (Integration of ice-core, marine and terrestrial records) and the Subcommission on Quaternary Stratigraphy (International Commission on Stratigraphy), J. Quat. Sci., 27(7), 649–659, doi:10.1002/jqs.2565, 2012.

Wang, Y., Cheng, H., Edwards, R. L., An, Z., Wu, J., Shen, C.-C. and Dorale, J. A.: A high-resolution absolute-dated late Pleistocene Monsoon record from Hulu Cave, China., Science, 294(5550), 2345–8, doi:10.1126/science.1064618, 2001.

Wang, Y., Cheng, H., Edwards, R. L., He, Y., Kong, X., An, Z., Wu, J., Kelly, M. J., Dykoski, C. A. and Li, X.: The Holocene Asian monsoon: links to solar changes and North Atlantic climate.,

Science, 308(5723), 854–857, doi:10.1126/science.1106296, 2005.

Wang, Y., Cheng, H., Edwards, R. L., Kong, X., Shao, X., Chen, S., Wu, J., Jiang, X., Wang, X. and An, Z.: Millennial- and orbital-scale changes in the East Asian monsoon over the past 224,000 years., Nature, 451(7182), 1090–1093, doi:10.1038/nature06692, 2008.

Wu, B. and Wang, J.: Winter Arctic Oscillation, Siberian High and East Asian Winter Monsoon, Geophys. Res. Lett., 29(19), 3-1-3–4, doi:10.1029/2002GL015373, 2002.

Xue, F., Wang, H. and He, J.: Interannual Variability of Mascarene High and Australian High and Their Influences on East Asian Summer Monsoon, J. Meteorol. Soc. Japan, 82(4), 1173–1186, doi:10.2151/jmsj.2004.1173, 2004.

Yu, J., Anderson, R. F., Jin, Z., Rae, J. W. B., Opdyke, B. N. and Eggins, S. M.: Responses of the deep ocean carbonate system to carbon reorganization during the Last Glacial–interglacial cycle, Quat. Sci. Rev., 76, 39–52, doi:10.1016/j.quascirev.2013.06.020, 2013.

Yu, Y., Yang, T., Li, J., Liu, J., An, C., Liu, X., Fan, Z., Lu, Z., Li, Y. and Su, X.: Millennial-scale Holocene climate variability in the NW China drylands and links to the tropical Pacific and the North Atlantic, Palaeogeogr. Palaeoclimatol. Palaeoecol., 233(1–2), 149–162, doi:10.1016/j.palaeo.2005.09.008, 2006.

Yuan, D., Cheng, H., Edwards, R. L., Dykoski, C. A., Kelly, M. J., Zhang, M., Qing, J., Lin, Y., Wang, Y., Wu, J., Dorale, J. A., An, Z. and Cai, Y.: Timing, duration, and transitions of the last interglacial Asian monsoon., Science, 304(5670), 575–578, doi:10.1126/science.1091220, 2004.

Zijderveld, J. D. A.: A. C. demagnetization of rocks : analysis of results, in Methods in Palaeomagnetism, edited by D. W. Collinson, K. M. Creer, and S. K. Runcorn, pp. 254–286, Elsevier., 1964.

Captions

Table 1. AMS ^{14}C data in monospecies planktic foraminifera *N. pachyderma* sin. and benthic foraminifera *Epistominella pacifica* and *Uvigerina parvocostata* of core 41-2. All measured AMS ^{14}C data were calibrated by Calib 6.0 (Stuiver and Reimer, 1993) with Marine13 calibration curve (Reimer et al., 2013) with a surface water reservoir ages of 900 years (Max et al., 2014). In case of using benthic foraminifera for dating, we accept difference in paired benthic-planktic foraminifera ages equals to 1,400 years, based on unpublished data and total regional results of Max et al. (2014). All radiocarbon ages were converted into calibrated 1-sigma calendar age.

#	Lab. code	core depth cm	foraminifera species	14C-age year	Err.1 sigma year	calendar age, ka
1	YAUT-021713	120	*E. pacifica*	10078	47	9.121
2	YAUT-021714	127.5	*E. pacifica*	10340	42	9.445
3	UCIAMS-148095	298	*N. pachyd.*	13160	50	14.393
4	UCIAMS-148096	156	*Uv. parvoc.*	11135	45	10.60
5	UCIAMS-148098	306	*Uv. parvoc.*	14185	35	14.616

884 Table 2. Centennial events with increased / decreased productivity during 25-8 ka in core 41-2 and
885 the average ages according to the correlations between productivity events and the EASM sub-
886 interstadials and sub-stadials (CsI/CsS).

887

Events	Core interval, cm	Averaged cal. age, ka
CsS-EH-1	105-110	8.2
CsI-EH-1	111-116	8.6
CsS-EH-2	117-123	9.1
CsI-EH-2	124-129	9.5
CsS-EH-3	131-140	9.9
CsI-EH-3	141-153	10.5
CsS-EH-4	155-167	11.1
CsI-EH-4	168-181	11.5
CsI-GI1-a	231-238	13.1
CsI-GI1-c1	248-262	13.5
CsI-GI1-c3	269-279	13.8
CsI-GI1-e	285-306	14.3
CsI-GS2.1-1	317-322	14.9
CsI-GS2.1-2	335-339	15.5
CsI-GS2.1-3	353-360	16.5
CsI-GS2.1-4	373-381	17.5
CsI-GS2.1-5	388-395	18.1
CsI-GS2.1-6	399-407	18.6
CsI-GS2.1-7	420-425	19.2
CsI-GS2.1-8	432-437	19.5

888

889

890

Table 3. The age controlling points of core 41-2 is derived from available AMS ^{14}C data of core 41-2, projection AMS 14C age of core 12KL, and tie points through correlation between increased productivity events and EASM CsIs (Wang et al., 2008). One AMS ^{14}C datum of core 12KL at depth of 706 cm was accepted according to the Tiedemann/Max age model 2 (Max et al., 2012, 2014).

Depth	AMS 14C core 41-2	Key time points of core 12KL	correlation with ages of China subInterstadial	Accepted key time points
cm	Cal. age, ka	ka/ depth (cm)		Cal. age, ka
120	9.12			9.12
127.5	9.45			
126		9.51/210		9.51
156	10.6			
159		11.08/295		11.08
167		11.31/340		11.31
234			13.08/GsI-GI1-a	13.08
251		13.42/508		13.42
273		13.79/550		13.79
298	14.39			
303		14.42/611		14.42
306	14.61			
337			15.42/CsI-GS2.1-2	15.42
348		16.16/706		16.16
357			16.51/ CsI-GS2.1-3	16.51
379			17.56/ CsI-GS2.1-4	17.56
393			18.12/ CsI-GS2.1-5	18.12
402		18.6/821		18.6
405			18.78/ CsI-GS2.1-6	18.78
423			19.25/ CsI-GS2.1-7	19.25
434		19.54/876		19.54

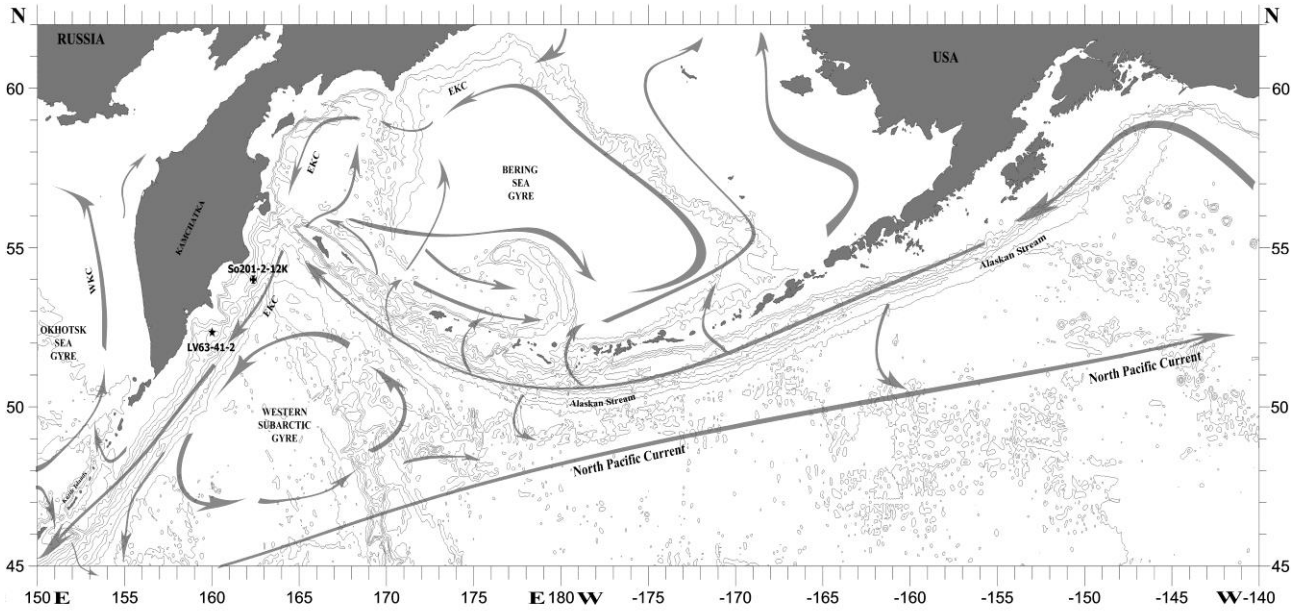

Fig. 1. Bathymetry, surface water currents and location of the cores 41-2 (star) and 12KL (cross) (Max et al., 2012) in the N Pacific. Surface currents as in (Favorite et al., 1976) with modifications. EKC – East Kamchatka Current, WKC – West Kamchatka Current.

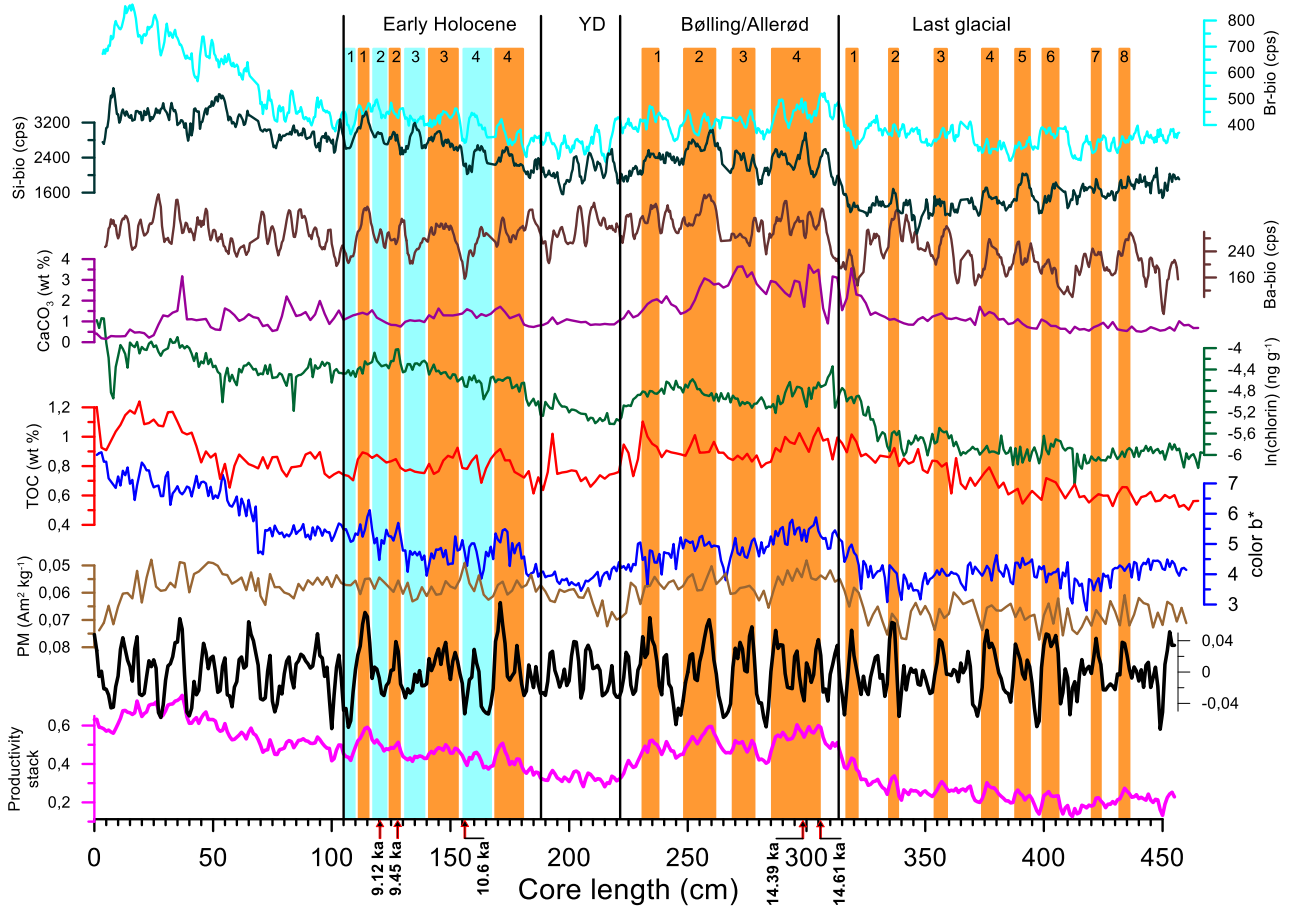

Fig. 2. Records (from bottom to top) of the original and detrended productivity stacks, PM, color b*, TOC, chlorin, $CaCO_3$, Ba-bio, Si-bio, and Br-bio versus depth. Preliminary boundaries of the B/A warming, YD cooling, and Holocene are shown according to general variability of productivity in the NW Pacific, Sea of Okhotsk, and Bering Sea (Galbraith et al., 2007; Gorbarenko, 1996; Gorbarenko and Goldberg, 2005; Keigwin, 1998; Seki et al., 2004). AMS ^{14}C data (calendar ka) were shown at the base. Blue bars indicate cold periods / lower productivity events. Orange bars indicate warm periods / high producitivity events.

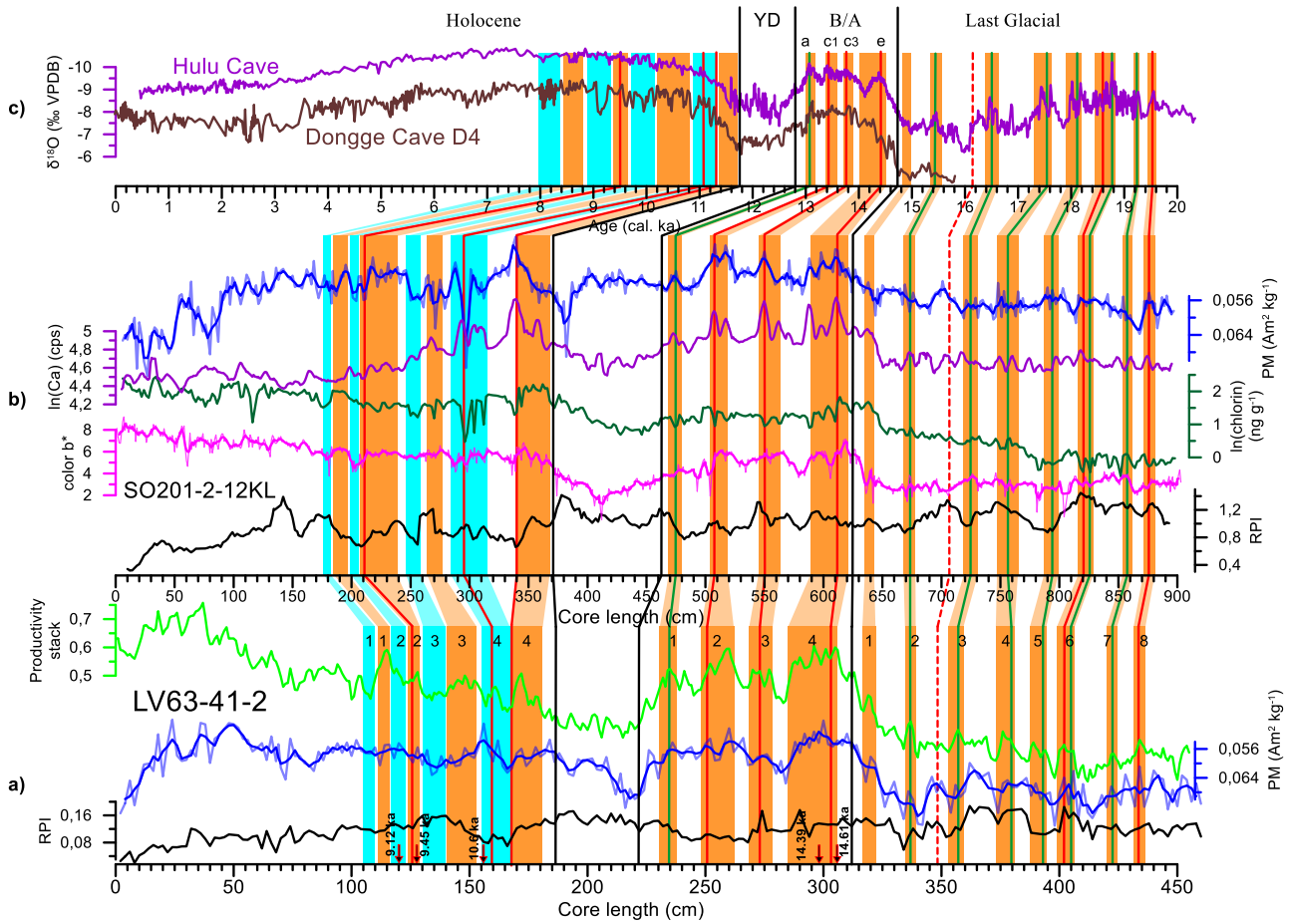

Fig. 3. Age model of core 41-2. Low panel: (a) RPI, PM and productivity stack of core 41-2 versus depth. (b) Middle panel: RPI, color b*, chlorin, Ca and PM of core 12KL versus depth. (c) Upper panel: $\delta^{18}O$ calcite of Chinese cave stalagmites (Dykoski et al., 2005; Wang et al., 2008) over the last 20 ka. The correlation of productivity events between core 41-2 and 12KL was established according to correlation of productivity stack of core 41-2 with productivity proxies of core 12KL and the RPI records of both cores. AMS ^{14}C data of core 12KL (red lines) were projected to the core 41-2 according to correlated productivity events. A close correlation of the productivity events with sub-interstadials in the EASM becomes apparent after projection of the radiocarbon data on the age scale of EASM. Green lines correlate EASM sub-interstadials with productivity events. Orange and blue bars are as in Fig. 2.

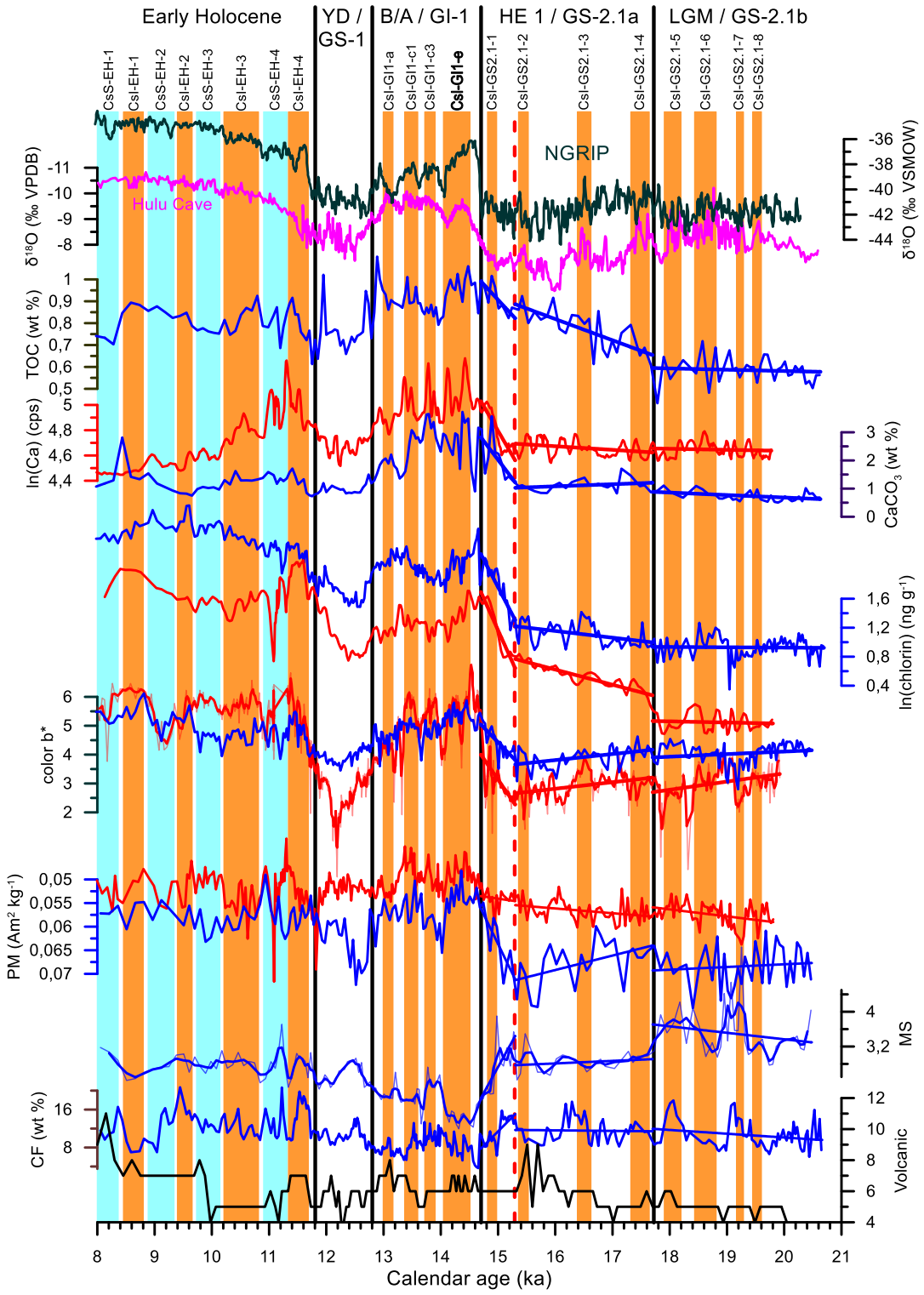

927

928 Fig. 4. High resolution variability of the productivity and lithologic proxies in the NW Pacific
929 during 21–8 ka. Volcanic particles, CF, MS, PM, color b*, chlorin, $CaCO_3$/Ca, and TOC
930 determined in cores 41-2 (blue lines) and 12KL (red lines) are shown from bottom to top. Δ18O
931 records of EASM (Wang et al., 2008) and NGRIP (North Greenland Ice Core Project members,
932 2004) are shown at the top of the figure. Linear trends are shown for productivity and lithologic
933 proxies during 20-17.8, 17.8-15.3, and 15.3-14.7 ka periods. Red dashed line marks the boundary in
934 productivity and lithologic trends during HE1 at 15.3 kyr. Orange and blue bars are as in Fig. 2.

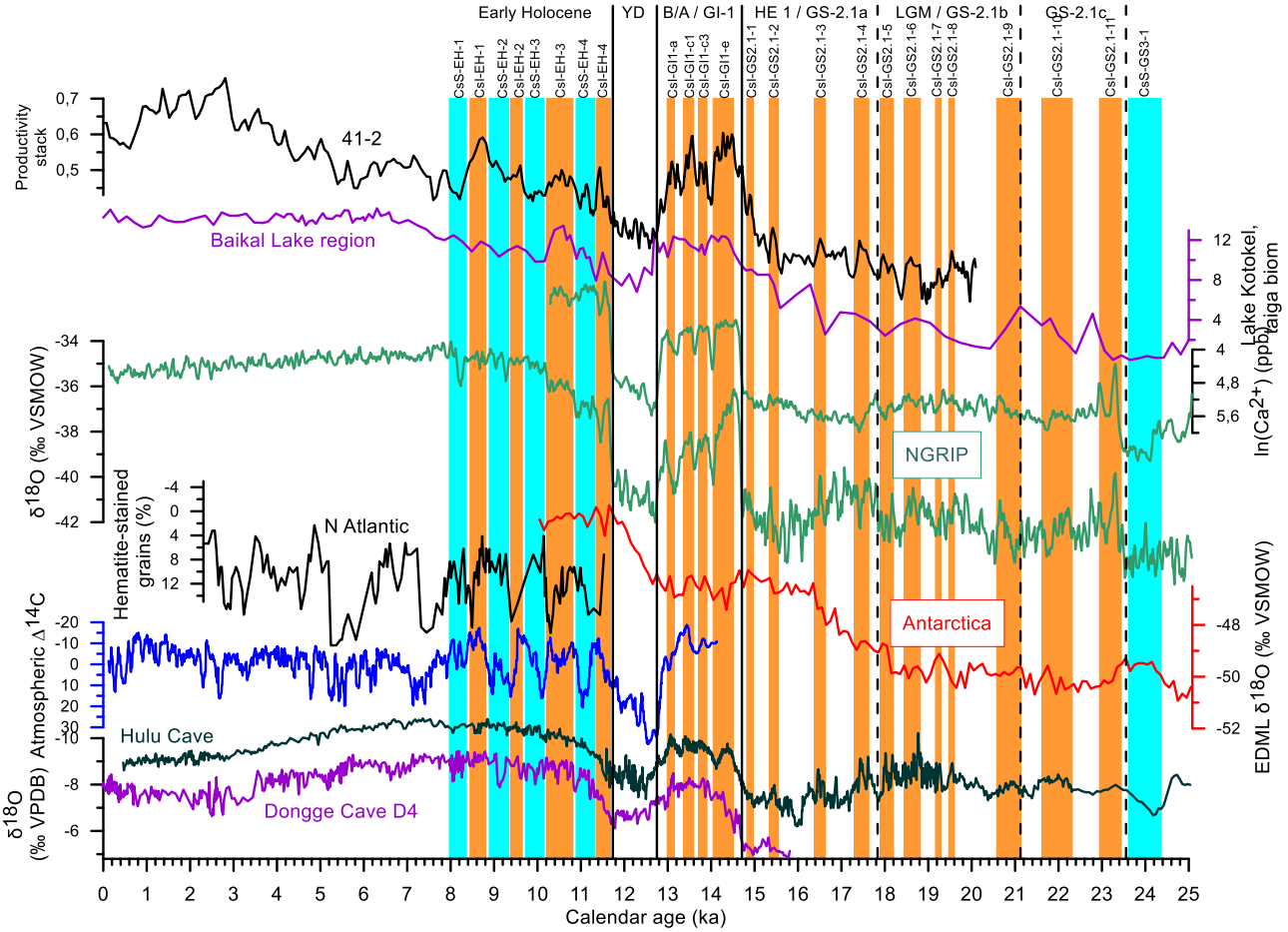

Fig. 5. Compilations of Northern and Southern Hemisphere climate records, solar activity, NW Pacific productivity events, and vegetation records from the southern Siberia during the last 25 ka. From bottom to top: absolutely dated $\delta^{18}O$ calcite of Chinese cave stalagmites (Dykoski et al., 2005; Wang et al., 2008); the residual atmospheric $\Delta^{14}C$ record of around 2000-year moving average (Reimer et al., 2004); $\delta^{18}O$ EDML records after methane synchronization with the N Greenland ice core (EPICA Community Members, 2006); the petrologic tracer of drift ice in the N Atlantic (Bond et al., 2001); the $\delta^{18}O$ and Ca^{2+} records in the Greenland NGRIP ice core indicated air temperature and dust variability on GICC05 age scale (Rasmussen et al., 2014), pollen reconstructed Southern Siberia environment changes (Lake Baikal region) (Bezrukova et al., 2010) and productivity stack for core 41-2. Orange and blue bars are as in Fig. 2. Centennial events with increased productivity are associated with sub-interstadial of the EASM and with increasing input of solar irradiance during the LGM-B/A and EH short-term warmings, respectively. The correlation between short-term increased Greenland temperature (NGRIP ice core) and a decreased Antarctic temperature is less pronounced but seems to be marked as well.

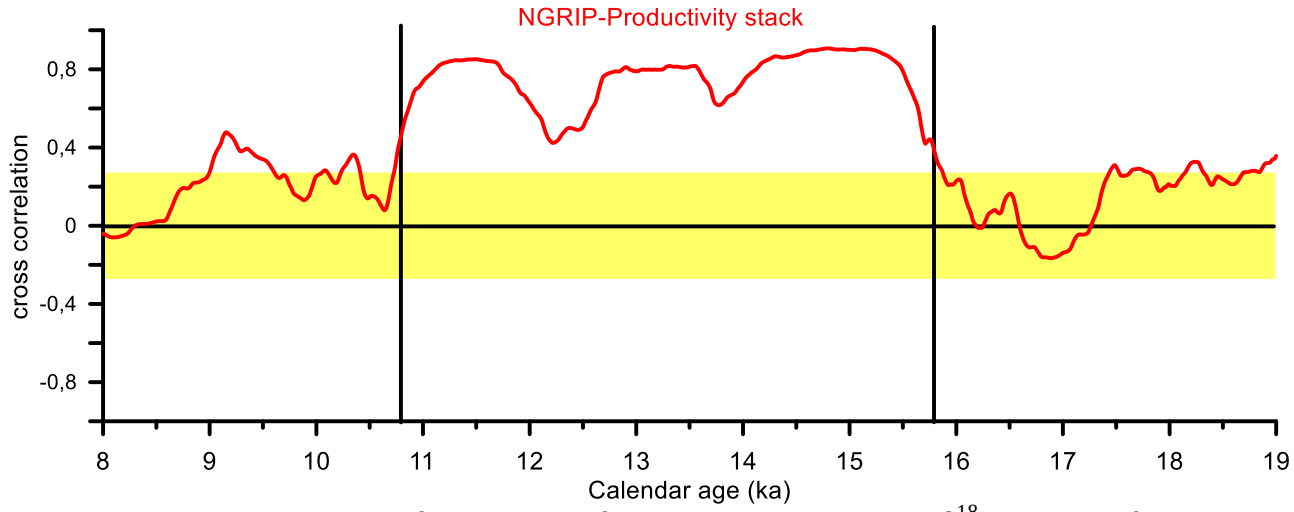

Fig. 6. Cross correlation (CC) of the NW Pacific productivity stack and $\delta^{18}O$ records of the NGRIP (Rasmussen et al., 2014), using moving windows at 2000 years. Yellow bars depict the CC within range ±0.25. Vertical black lines distinguish an interval from 10.8 to 15.8 ka with significant CC (from -0.6 to -0.9) from less significant CC during earlier and later intervals indicating the synchronicity climate changes between the N Atlantic and NW Pacific.